Journal of Solid State Chemistry 183 (2010) 829–843

Contents lists available at ScienceDirect

Journal of Solid State Chemistry

journal homepage: www.elsevier.com/locate/jssc

The ternary system cerium–rhodium–silicon

Alexey Lipatov [a,b], Alexander Gribanov [a,c,*], Andriy Grytsiv [a], Sergey Safronov [c], Peter Rogl [a], Julia Rousnyak [c], Yurii Seropegin [c], Gerald Giester [d]

[a] Institute of Physical Chemistry, University of Vienna, Währingerstrasse 42, A-1090 Wien, Austria
[b] Materials Science Department of the Moscow State University, Leninskie Gory 1, GSP-1, 119991 Moscow, Russia
[c] Chemistry Department of the Moscow State University, Leninskie Gory 1, GSP-1, 119991 Moscow, Russia
[d] Institute of Mineralogy and Crystallography, University of Vienna, Althanstrasse 14, A-1090 Wien, Austria

ARTICLE INFO

Article history:
Received 29 November 2009
Received in revised form
27 January 2010
Accepted 30 January 2010
Available online 4 February 2010

Keywords:
Ternary system Ce–Rh–Si
Ternary silicides
Phase equilibria at 800 °C
X-ray single crystal and powder diffraction

ABSTRACT

Phase relations have been established in the ternary system Ce–Rh–Si for the isothermal section at 800 °C based on X-ray powder diffraction and EPMA on about 80 alloys, which were prepared by arc melting under argon or by powder reaction sintering. From the 25 ternary compounds observed at 800 °C 13 phases have been reported earlier. Based on XPD Rietveld refinements the crystal structures for 9 new ternary phases were assigned to known structure types. Structural chemistry of these compounds follows the characteristics already outlined for their prototype structures: τ_7—Ce_3RhSi_3, ($Ba_3Al_2Ge_2$-type), τ_8—$Ce_2Rh_{3-x}Si_{3+x}$ ($Ce_2Rh_{1.35}Ge_{4.65}$-type), τ_{10}—$Ce_3Rh_{4-x}Si_{4+x}$ ($U_3Ni_4Si_4$-type), τ_{11}—$CeRh_6Si_4$ ($LiCo_6P_4$-type), τ_{13}—$Ce_6Rh_{30}Si_{19.3}$ ($U_6Co_{30}Si_{19}$-type), τ_{18}—$Ce_4Rh_4Si_3$ ($Sm_4Pd_4Si_3$-type), τ_{21}—$CeRh_2Si$ ($CeIr_2Si$-type), τ_{22}—$Ce_2Rh_{3+x}Si_{1-x}$ (Y_2Rh_3Ge-type) and τ_{24}—$Ce_8(Rh_{1-x}Si_x)_{24}Si$ ($Ce_8Pd_{24}Sb$-type). For τ_{25}—$Ce_4(Rh_{1-x}Si_x)_{12}Si$ a novel *bcc* structure was proposed from Rietveld analysis. Detailed crystal structure data were derived for τ_3—$CeRhSi_2$ ($CeNiSi_2$-type) and τ_6—$Ce_2Rh_3Si_5$ ($U_2Co_3Si_5$-type) by X-ray single crystal experiments, confirming the structure types. The crystal structures of τ_4—$Ce_{22}Rh_{22}Si_{56}$, τ_5—$Ce_{20}Rh_{27}Si_{53}$ and τ_{23}—$Ce_{33.3}Rh_{58.2-55.2}Si_{8.5-11.5}$ are unknown. High temperature compounds with compositions $Ce_{10}Rh_{51}Si_{33}$ ($U_{10}Co_{51}Si_{33}$-type) and CeRhSi (LaIrSi-type) have been observed in as-cast alloys but these phases do not participate in the phase equilibria at 800 °C.

© 2010 Elsevier Inc. All rights reserved.

1. Introduction

Six ternary compounds from the title system, $CeRh_2Si_2$ ($ThCr_2Si_2$-type) [1], $CeRhSi_3$ ($BaNiSn_3$-type) [2,3], $CeRhSi_2$ ($CeNiSi_2$-type), $CeRh_3Si_2$ ($CeCo_3B_2$-type), $Ce_2Rh_3Si_5$ ($U_2Co_3Si_5$-type) [4] and Ce_2RhSi_3 (Er_2RhSi_3-type) [5] were described prior to the first investigation of the entire Ce–Rh–Si phase diagram at 600 °C by Shapiev [6]. In his work 17 ternary compounds were found, however, only the approximate composition for 11 new compounds was derived from phase analysis on X-ray powder photographs: $Ce_{10}Rh_{75}Si_{15}$, $Ce_{10}Rh_{60}Si_{30}$, $Ce_{10}Rh_{55}Si_{35}$, $Ce_{27.5}Rh_{43.5}Si_{29}$, $Ce_{33.3}Rh_{56.3}Si_{10}$, $Ce_{33.3}Rh_{46.7}Si_{20}$, $Ce_{33.3}Rh_{33.3}Si_{33.4}$, $Ce_{33.3}Rh_{26.3}Si_{40}$, $Ce_{40}Rh_{15}Si_{45}$, $Ce_{45}Rh_{25}Si_{30}$, $Ce_{51.5}Rh_{40}Si_{8.5}$. Since 1993 additional knowledge has been acquired and crystal structures of several ternary phases were determined, i.e. $Ce_6Rh_{30}Si_{19}$ ($Sc_6Co_{30}Si_{19}$-type) [7], $Ce_2Rh_{12}Si_7$ ($Ho_2Rh_{12}As_7$-type) [7], $Ce_2Rh_{15}Si_7$ (own-type) [8], $Ce_3Rh_3Si_2$ (own-type) [9], $CeRh_2Si$ (inverse $CeNiSi_2$-type) [10], $Ce_3Rh_2Si_2$ ($La_3Ni_2Ga_2$-type) [11]. More accurate version of the crystal structure was established for $CeRh_3Si_2$ ($ErRh_3Si_2$-type—an orthorhombic superstructure of $CeCo_3B_2$ [12]) and for Ce_2RhSi_3 (Er_2RhSi_3-type) a higher symmetry from $P\bar{6}2c$ to $P6_3/mmc$ was proposed [13]. Physical properties of several compounds from the Ce–Rh–Si system were investigated and revealed interesting electrical and/or magnetic anomalies, such as heavy-fermion behavior (including non-centrosymmetric heavy-fermion superconductivity in $CeRhSi_3$—see [14] and for latest investigations [15–20]) and/or Kondo-lattices as well as valence instabilities, e.g. for $CeRh_2Si_2$ [21–33], $CeRhSi_2$ [34–36], Ce_2RhSi_3 [5,37–42], $CeRh_2Si$ [43,44], $Ce_2Rh_3Si_5$ [45,46], $CeRh_3Si_2$ [47–49], $Ce_3Rh_3Si_2$ [50] and $Ce_2Rh_2Si_5$ [51] (for the latter phase no crystal structure data were given). Physical properties of four compounds with known crystal structure, i.e. $Ce_2Rh_{15}Si_7$, $Ce_2Rh_{12}Si_7$, $Ce_6Rh_{30}Si_{19}$ and $Ce_3Rh_2Si_2$, have not been reported yet.

As the early data presented by Shapiev [6] do not fully comply with information hitherto given, we reinvestigated the phase equilibria in the Ce–Rh–Si system. In the present paper we provide comprehensive knowledge on the phase equilibria at 800 °C and crystal structures of intermetallics. The annealing temperature of 800 °C was chosen in order to achieve enhanced

* Corresponding author at: Chemistry Department of the Moscow State University, Leninskie Gory 1, GSP-1, 119991 Moscow, Russia.
Fax: +7 495 939 0171.
E-mail address: avgri@mail.ru (A. Gribanov).

0022-4596/$ - see front matter © 2010 Elsevier Inc. All rights reserved.
doi:10.1016/j.jssc.2010.01.029

Table 1
Crystallographic data of solid phases in the Ce–Rh–Si system.

Phase	Space group	Lattice parameters (nm)			Comments
Temperature range (°C)	Prototype	*a*	*b*	*c*	
(δCe)	$Im\bar{3}m$	0.412			[67]
798–726 [67]	*W*				
(γCe)	$Fm\bar{3}m$	0.51610			[67]
726–61 [67]	*Cu*				
(βCe)	$P6_3/mmc$	0.36810		1.1857	[67]
61–(−177) [67]	*αLa*				
(αCe)	$Fm\bar{3}m$	0.485			[67]
≤ −177 [67]	*Cu*				
(Rh)	$Fm\bar{3}m$	0.38032			[67]
≤ 1963 [67]	*Cu*				
(Si)	$Fm\bar{3}m$	0.54306			[67]
≤ 1414 [67]	*C (diamond)*				
Ce_5Si_3	*I4/mcm*	0.7868		1.373	[68]
≤ 1260 [59]	Cr_5B_3	0.7878		1.367	[59]
$Ce_5(Si_{1-x}Rh_x)_3$					$0 \le x \le 0.3$ [69] at 600 °C
		0.7873		1.3796	x=0.15 [69] at 600 °C
		0.78592		1.3657	x_{max}=0.3 [69] at 600 °C
Ce_3Si_2	*P4/mbm*	0.7780		0.4367	[59]
≤ 1335 [59]	U_3Si_2	0.77908(4)		0.43690(3)	[d]
Ce_5Si_4	$P4_12_12$	0.7936		1.5029	[59]
≤ 1500 [59]	Zr_5Si_4	0.79438(3)		1.5098(1)	[d]
CeSi	*Pnma*	0.8298	0.3961	0.5959	[59]
≤ 1630 [59]	FeB	0.82832(3)	0.39756(1)	0.59601(2)	[d]
$CeSi_{1.34}$	*Cmcm* V_2B_3 (Nd_2Si_{3-x})	0.44035	2.48389	0.39517	[60] at 35 K
$CeSi_{1.67}$	*Imma*	0.4109	0.4189	1.3917	Si-saturated (sat.) [59]
≤ 1725 [59]	$GdSi_{2-x}$	0.4190	0.4113	1.3906	Rh-sat. [59]
		0.41220(1)	0.41913(1)	1.3914(1)	[d]
$CeSi_{2-x}$	$I4_1/amd$	0.4192		1.3913	x=0 [59]
≤ 1575 [59]	$ThSi_2$	0.41897(3)		1.3932(1)	x=0[d]
$Ce(Si_{1-y}Rh_y)_{2-x}$		0.41907(1)		1.3937(1)	x=0, y=0.06[d]
		0.41845(1)		1.4025(1)	x=0, y=0.105[d]
		0.41781(1)		1.4138(1)	x=0, y_{max}=0.144[d]
Ce_7Rh_3	$P6_3mc$	1.0051		0.6378	[61]
≤ 755 [61]	Th_7Fe_3	1.0005		0.6356	[70]
		1.0023		0.6376	[71]
Ce_5Rh_3	*P4/ncc*	1.1260		0.6450	[61]
≤ 725 [61]	Pu_5Rh_3				
Ce_3Rh_2	$R\bar{3}$	0.8858		1.6794	[61]
≤ 815 [61]	Er_3Ni_2	0.8835		1.676	[72]
Ce_5Rh_4	*Pnma*	0.7467	1.4841	0.7624	[61]
≤ 955 [61]	Sm_5Ge_4	0.7434	1.486	0.7604	[73]
		0.7486(1)	1.4788(2)	0.7657(1)	[d]
CeRh	*Cmcm*	0.3845	1.0964	0.4174	[61]
≤ 1055 [61]	CrB	0.3852	1.0986	0.4152	[74]
		0.3855	1.0966	0.4153	[75]
		0.3844(1)	1.0946(2)	0.4174(1)	[d]
$CeRh_2$	*Fd* $\bar{3}m$	0.7545			Alloy at 65 at% Rh [61]
≤ 1450[61]	$MgCu_2$	0.7543			Alloy at 70 at% Rh [61]
		0.7538			[76]
		0.7547			Ce-sat. [76]
		0.7534			Rh-sat. [76]
		0.7550			[77]
		0.7539			[78]
		0.75387(2)			Rh-sat.[d]
$Ce(Rh_{1-x}Si_x)_2$					$0 \le x \le 0.10$[d]
		0.75256(2)			x=0.04[d]
		0.75220(5)			x_{max}=0.10[d]
$CeRh_3$	$Pm\bar{3}m$	0.4022			Alloy at 70 at% Rh [61]
≤ 1550 [61]	Cu_3Au	0.4023			[79]
		0.4012			[70]
		0.4020			[76]
		0.4024			[80]
$CeRh_3Si_{1-x}$					$0.81 \le x \le 1.00$[d]
		0.40455(1)			x=0.91[d]
		0.40616(1)			x=0.87[d]
		0.40912(1)			x_{min}=0.81[d]
Rh_2Si	*Pnma*	0.5404	0.3930	0.7390	[81]
≤ 1622 [62]	αCo_2Si	0.54109(1)	0.39294(1)	0.73855(1)	[d]
Rh_5Si_3	*Pbam*	0.5322	1.0126	0.3897	[81]
≤ 1470 [62]	Rh_5Ge_3	0.53181(1)	1.01257(2)	0.38966(1)	[d]
$Rh_{20}Si_{13}$	$P6_3/m$	1.1851		0.3623	[82]
1050 – 1225 [62]	$Rh_{20}Si_{13}$	1.1853(1)		0.36128(1)	[d]

Table 1 (*continued*)

Phase	Space group	Lattice parameters (nm)			Comments
Temperature range (°C)	Prototype	*a*	*b*	*c*	
Rh_3Si_2	$P\bar{3}m1$	0.3965		0.5051	[81]
metastable [62]	Rh_3Si_2				
αRhSi	*Pnma*	0.5545	0.3067	0.6376	Rh-sat. 49.8 at% Si [81]
≤1030 [62] Si-sat.	MnP	0.555	0.3084	0.6350	Si-sat. 50.7 at% Si [81]
≤1080 [62] Rh-sat.		0.55466(5)	0.30707(2)	0.63658(5)	Si-sat. 50 at% Rh[d]
		0.55517(3)	0.30707(1)	0.63736(3)	Rh-sat. 50.8 at% Rh[d]
βRhSi	$P2_13$	0.4685			Rh-sat. 49.8 at% Si [81]
1030–1452 [62]	FeSi	0.4674			Si-sat. 50.7 at% Si [81]
Si-sat.		0.46822(2)			Rh-sat.[d] as-cast
1080–1452 [62]					
Rh-sat.					
Rh_4Si_5	$P12_1/m$	1.234	0.3512	0.5929	[81]
≤1030 [62]	Rh_4Si_5		β=100.18°		
		1.2335(1)	0.35071(2)	0.59285(4)	[d]
			β=100.18(1)°		
Rh_3Si_4	*Pnma*	1.880	0.3613	0.5808	[81]
≤1040 [62]	Rh_3Si_4	1.8800(1)	0.36048(2)	0.58089(3)	[d]
τ_1, $CeRhSi_3$	*I4mm*				[2,3]
	$BaNiSn_3$	0.4204		0.974	[34]
		0.4269		0.9738	[83]
		0.4240		0.9801	[84]
		0.4235		0.9788	[85]
		0.4244		0.9813	[17]
		0.4237		0.9760	[20]
		0.42311(1)		0.97816(3)	[d]
τ_2, Ce_2RhSi_3	$P6_3/mmc$				[5,13]
	Er_2RhSi_3	0.8262		0.8439	[37]
		0.8327		0.8516	[39]
		0.8240		0.8444	[40]
		0.8237		0.8445	[41]
$Ce_2Rh_{1-x}Si_{3+x}$					$0 \le x \le 0.24$[d]
		0.82359(2)		0.84212(3)	x_{min}=0[d]
		0.82255(1)		0.84605(1)	x=0.10[d]
		0.82162(1)		0.84804(2)	x=0.18[d]
		0.82068(1)		0.85030(2)	x_{max}=0.24[d]
τ_3, $CeRhSi_2$	*Cmcm*	0.42661	1.6758	0.41708	[34]
	$CeNiSi_2$	0.4289	1.6805	0.4232	[35]
		0.4310	1.6743	0.4216	[36]
$CeRh_{1-x}Si_{2+x}$					$0 \le x \le 0.32$[d]
		0.42629(1)	1.67456(3)	0.41731(1)	x_{min}=0.0[d]
		0.42582(1)	1.67526(2)	0.41773(1)	x=0.15[d]
		0.42604(2)	1.67737(6)	0.41787(1)	x=0.24[d] SC
		0.42566(4)	1.6768(2)	0.41763(4)	x_{max}=0.32[d]
τ_4, $Ce_{22}Rh_{22}Si_{56}$	Unknown				[d]
$Ce_2Rh_2Si_5$					[51]
τ_5, $Ce_{20}Rh_{27}Si_{53}$[a]	t^{**}	0.41391(1)		0.99650(2)	[d]
	$BaAl_4$-deriv.				
τ_6, $Ce_2Rh_3Si_5$	*Ibam*	0.9874	1.183	0.5822	[86]
	$U_2Co_3Si_5$	0.989	1.187	0.582	[46]
		0.99118(2)	1.17558(3)	0.58313(1)	[d]SC
τ_7, Ce_3RhSi_3	*Immm*	0.41528(1)	0.42548(1)	1.81906(5)	[d]
	$Ba_3Al_2Ge_2$				
τ_8, $Ce_2Rh_{3-x}Si_{3+x}$	*Pmmn*				$0.05 \le x \le 0.36$[d]
	$Ce_2Rh_{1.35}Ge_{4.65}$	0.41035(2)	0.41091(2)	1.72633(7)	x_{min}=0.05[d]
		0.41103(1)	0.41047(1)	1.72595(2)	x=0.27[d]
		0.41167(2)	0.40920(2)	1.72339(6)	x_{max}=0.36[d]
τ_9, $CeRh_2Si_2$	*I4/mmm*	0.4086		1.017	[1]
	$ThCr_2Si_2$	0.4093		1.0185	[21]
		0.4075		1.013	[23]
		0.40840		1.01693	T=47.5 K [22]
		0.40834		1.01713	T=32 K [22]
		0.40828		1.01705	T=10 K [22]
		0.409		1.018	r.t. [22]
		0.4087		1.017	[87]
		0.4088		1.0178	[47]
		0.40883(1)		1.01748(2)	[d]
τ_{10}, $Ce_3Rh_{4-x}Si_{4+x}$	*Immm*				$0.0 \le x \le 0.1$[d]
	$U_3Ni_4Si_4$	0.40676(1)	0.41409(1)	2.44727(4)	x_{min}=0[d]
		0.40813(2)	0.41322(2)	2.4465(1)	x_{max}=0.1[d]
τ_{11}, $CeRh_6Si_4$	$P\bar{6}m2$	0.69881(2)		0.37808(2)	[d]
	$LiCo_6P_4$				
τ_{12}, $CeRh_3Si_2$	*Imma*	0.7128	0.9725	0.5595	[47]
	$ErRh_3Si_2$	0.7125	0.9709	0.5592	[88] SC
		0.71121	0.96810	0.55828	[48] SC

Table 1 (*continued*)

Phase	Space group	Lattice parameters (nm)			Comments
Temperature range (°C)	Prototype	*a*	*b*	*c*	
		0.71252(1)	0.97220(2)	0.55932(1)	[d]
τ_{13}, $Ce_6Rh_{30}Si_{19.3}$	$P6_3/m$	2.2300(1)		0.38398(1)	[d]
	$U_6Co_{30}Si_{19}$				
τ_{14}, $Ce_6Rh_{30}Si_{19}$	$P6_3/m$	1.5698		0.38571	[7] SC
	$Sc_6Co_{30}Si_{19}$	1.57257(2)		0.38569(1)	[d]
τ_{15}, $Ce_2Rh_{12}Si_7$	$P6_3/m$	0.9706		0.38394	[7] SC
	$Ho_2Rh_{12}As_7$	0.97199(2)		0.38480(1)	[d]
τ_{16}, $Ce_2Rh_{15}Si_7$	$Pm\bar{3}m$	0.8818			[8] SC
	$Ce_2Rh_{15}Si_7$	0.88323(2)			[d]
τ_{17}, $Ce_3Rh_2Si_2$	*Pbcm*	0.56762	0.79718	1.3271	[11] SC
	$La_3Ni_2Ga_2$				
		0.56849(5)	0.79745(7)	1.3289(1)	[d]
τ_{18}, $Ce_4Rh_4Si_3$	*C*2/*c*	2.0749(1)	0.57242(3)	0.78741(3)	[d]
	$Sm_4Pd_4Si_3$		β=110.09(1)°		
τ_{19}, $Ce_3Rh_3Si_2$	*Pnma*	0.7722	1.4822	0.5759	[9] SC
	$Ce_3Rh_3Si_2$	0.77036	1.4848	0.57466	[50]
		0.77176(6)	1.4874(1)	0.57599(5)	[d]
τ_{20}, $CeRh_{1.88}Si_{1.12}$	*Cmcm*	0.40591(3)	1.7673(1)	0.40736(3)	[d]
	inv.-$CeNiSi_2$	0.40413	1.7730	0.40675	SC for $CeRh_2Si$ [10]
τ_{21}, $CeRh_{2-x}Si_{1+x}$	$I4_1/amd$				$0.0 \le x \le 0.1$[d]
	$CeIr_2Si$ [64]	0.40521(2)		3.5556(2)	$x_{min}=0$[d]
		0.40560(4)		3.5472(4)	$x_{max}=0.1$[d]
τ_{22}, $Ce_2Rh_{3+x}Si_{1-x}$	$R\bar{3}m$				$0.08 \le x \le 0.17$[d]
	Y_2Rh_3Ge	0.55577(2)		1.17766(6)	$x_{min}=0.08$[d]
		0.55364(2)		1.19249(5)	$x_{max}=0.17$[d]
τ_{23}, $Ce_{33.3}Rh_{58.2-55.2}Si_{8.5-11.5}$	unknown	1.5260(2)	0.7539(1)	0.5523(2)	$Ce_{33.3}Rh_{55.2}Si_{11.5}$[d]
	o*P**	1.5284(1)	0.7536(1)	0.5512(1)	$Ce_{33.3}Rh_{55.7}Si_{11}$[d]
	UMn_2(lt)-deriv.	1.5354(3)	0.7530(1)	0.5496(1)	$Ce_{33.3}Rh_{56.7}Si_{10}$[d]
		0.5135(1)	0.7529(1)	0.5485(1)	$Ce_{33.3}Rh_{57.7}Si_9$[d,b]
τ_{24}, $Ce_8(Rh_{1-x}Si_x)_{24}Si$	$Pm\bar{3}m$				$0.07 \le x \le 0.10$[d]
	$Ce_8Pd_{24}Sb$	0.82166(3)			$x_{min}=0.07$[d]
		0.82601(1)			$x_{max}=0.10$[d]
τ_{25}, $Ce_4(Rh_{1-x}Si_x)_{12}Si$	$Im\bar{3}m$				$0.00 \le x \le 0.03$[d]
	$Ce_4Rh_{12}Si$	0.82155(1)			$x_{min}=0$
		0.82342(1)			$x_{max}=0.03$
τ_{26}, $Ce_{10}Rh_{51}Si_{33}$[c]	$P6_3/m$	2.9107(1)		0.38334(1)	[d]
> 800 °C	$U_{10}Co_{51}Si_{33}$				
τ_{27}, CeRhSi[c]	$P2_13$	0.6231(1)			[d]
> 800 °C	LaIrSi				

[a] Lattice parameters are given for $BaAl_4$-subcell.
[b] Lattice parameters are given for UMn_2(lt)-subcell.
[c] Phase detected in as-cast alloy but does not participate in phase equilibria at 800 °C.
[d] This work.

diffusion in the system combining elements with rather different melting points.

2. Experimental techniques

More than 80 alloys, each with a weight of 0.5 g, were prepared by argon arc-melting from high-purity elements (> 99.9 mass%) on a water-cooled copper hearth. To ensure homogenization, all alloys were re-melted three times. Part of each sample was vacuum-sealed in quartz tubes and annealed at 800 °C for 15–30 days before being quenched by dropping the capsules into cold water. In order to ensure that equilibrium conditions were achieved at this temperature, selected alloys were powdered, cold compacted and sintered at 800 °C for 1 week.

X-ray powder diffraction (XPD) data from as-cast and annealed alloys were collected from a Guinier-Huber 670 image plate system (Cu$K\alpha_1$; $8^\circ < 2\theta < 100^\circ$) and/or a STOE STADI P transmission diffractometer, equipped with a linear PSD (monochromatic Cu$K\alpha_1$-radiation; $10^\circ < 2\theta < 90^\circ$). Precise lattice parameters were calibrated against Ge as internal standard (a_{Ge}=0.5657906 nm) using program STOE-WinXpow [52].

Single crystals were mechanically isolated from crushed alloys. Inspection on an AXS-GADDS texture goniometer assured high crystal quality, unit cell dimensions and Laue symmetry of the specimens prior to X-ray intensity data collection on a four-circle Nonius Kappa diffractometer equipped with a CCD area detector and employing graphite monochromated Mo$K\alpha$ radiation (λ=0.071073 nm). Orientation matrix and unit cell parameters were derived using program DENZO [53]. No absorption corrections were necessary because of the rather regular crystal shape and small dimensions of the investigated specimens. The structures were solved by direct methods [54] and refined with the SHELXL-97 program [55]. Quantitative X-ray Rietveld refinements were performed with the FULLPROF program [56,57], employing internal tables for X-ray atomic form factors. Atom parameters were standardized with the aid of program STRUCTURE TIDY [58].

All as-cast and annealed samples were polished via standard procedures and have been examined by scanning electron microscopy (SEM). Phase compositions were determined via electron probe microanalyses (EPMA) on a Carl Zeiss LEO EVO 50XVP instrument with a Link EDX INCA Energy 450 system (Q-BSD detector).

3. Binary systems

The Ce–Si binary phase diagram is used from a recent investigation by Bulanova et al. [59] amended by data on the existence of Ce_2Si_{3-x} (x=0.32) [60]. We accepted the latest carefully re-investigated version of the Ce–Rh binary by Palenzona et al. [61]. The Rh–Si phase diagram is taken from the assessment of Schlesinger [62]. Crystallographic data pertinent to the Ce–Rh–Si system are summarized in Table 1. X-ray powder diffraction intensities for unary and binary phases reported in literature agree well with those observed in ternary Ce–Rh–Si alloys.

4. Results and discussion

4.1. Crystal structures of ternary phases

In the present investigation 25 ternary compounds were found to participate in the phase equilibria of the Ce–Rh–Si system at 800 °C (Fig. 1), 13 of which were already known earlier and were confirmed to exist by XPD phase analysis and EPMA measurements: τ_1—$CeRhSi_3$ ($BaNiSn_3$-type) [2,3], τ_2—Ce_2RhSi_3 (Er_2RhSi_3-type) [5], τ_3—$CeRhSi_2$ ($CeNiSi_2$-type) [34], τ_4—$Ce_{22}Rh_{22}Si_{56}$ ($Ce_2Rh_2Si_5$ in [51], structure unknown), τ_6—$Ce_2Rh_3Si_5$ ($U_2Co_3Si_5$-type) [45,46], τ_9—$CeRh_2Si_2$ ($ThCr_2Si_2$-type) [1], τ_{12}—$CeRh_3Si_2$ ($ErRh_3Si_2$-type) [4,48], τ_{14}—$Ce_6Rh_{30}Si_{19}$ ($Sc_6Co_{30}Si_{19}$-type) [7], τ_{15}—$Ce_2Rh_{12}Si_7$ ($Ho_2Rh_{12}As_7$-type) [7], τ_{16}—$Ce_2Rh_{15}Si_7$ (own type) [8], τ_{19}—$Ce_3Rh_3Si_2$ (own type) [9], τ_{20}—$CeRh_{1.88}Si_{1.12}$ (inverse $CeNiSi_2$-type) [10], and τ_{17}—$Ce_3Rh_2Si_2$ ($La_3Ni_2Ga_2$-type) [11].

4.1.1. New compounds with known structure types

Based on XPD Rietveld refinements the crystal structures of nine new compounds were assigned to known structure types (Table 1). The structural chemistry of these compounds follows the characteristics already outlined for the prototype structures and thus will not be discussed here: τ_7—Ce_3RhSi_3 ($Ba_3Al_2Ge_2$-type), τ_8—$Ce_2Rh_{3-x}Si_{3+x}$ ($Ce_2Rh_{1.35}Ge_{4.65}$-type), τ_{10}—$Ce_3Rh_{4-x}Si_{4+x}$ ($U_3Ni_4Si_4$-type), τ_{11}—$CeRh_6Si_4$ ($LiCo_6P_4$-type), τ_{13}—$Ce_6Rh_{30}Si_{19.3}$ ($U_6Co_{30}Si_{19}$-type), τ_{18}—$Ce_4Rh_4Si_3$ ($Sm_4Pd_4Si_3$-type), τ_{21}—$CeRh_{2-x}Si_{1+x}$ ($CeIr_2Si$-type), τ_{22}—$Ce_2Rh_{3+x}Si_{1-x}$ (Y_2Rh_3Ge-type) and τ_{24}—$Ce_8(Rh_{1-x}Si_x)_{24}Si$ ($Ce_8Pd_{24}Sb$-type). The lattice parameters for these compounds and their homogeneity regions are summarized in Table 1. Results of Rietveld refinements of some of the aforementioned compounds are listed in Tables 2–5 with residual values being generally below $R_F < 0.059$: τ_8—$Ce_2Rh_{3-x}Si_{3+x}$ (at x=0.27), τ_{10}—$Ce_3Rh_{4-x}Si_{4+x}$ (at x=0) and τ_{11}—$CeRh_6Si_4$ (Table 2); τ_{13}—$Ce_6Rh_{30}Si_{19.3}$ (Table 3); τ_{17}—$Ce_3Rh_2Si_2$, τ_{18}—$Ce_4Rh_4Si_3$ and τ_{22}—$Ce_2Rh_{3+x}Si_{1-x}$ (at x=0.15) (Table 4); τ_{24}—$Ce_8(Rh_{1-x}Si_x)_{24}Si$ (at x=0.09) (Table 5).

The ternary phases τ_{11}–τ_{15} are forming in a narrow composition range (see inset in Fig. 1). EPMA analysis of the as-cast alloy $Ce_8Rh_{55}Si_{37}$ reveals four compositions (Fig. 2c), three of which were attributed to known phases by X-ray measurements: high temperature βRhSi, $Rh_{20}Si_{13}$ and τ_{11}—$CeRh_6Si_4$. The fourth phase X (Fig. 2c) has the composition $Ce_{10.5}Rh_{54.4}Si_{35.1}$. In spite of proximity to τ_{14}—$Ce_6Rh_{30}Si_{19}$, the X-ray pattern of $Ce_8Rh_{55}Si_{37}$ alloy does not show any trace of τ_{14}. Instead, reflections of two new compounds were detected: τ_{13}—$Ce_6Rh_{30}Si_{19.3}$ and τ_{26}—$Ce_{10}Rh_{51}Si_{33}$ with structure types of $U_6Co_{30}Si_{19}$ and $U_{10}Co_{51}Si_{33}$, respectively. Together with the structures of τ_{14}—$Ce_6Rh_{30}Si_{19}$ ($Sc_6Co_{30}Si_{19}$-type), τ_{15}—$Ce_2Rh_{12}Si_7$ ($Ho_2Rh_{12}As_7$-type) and the newly found phase τ_{11}—$CeRh_6Si_4$ ($LiCo_6Si_4$-type) all these structures are members of a hexagonal structure series with linked triangular columns following the general formula $Ce_{n(n+1)}Rh_{6(n^2+1)}Si_{4n^2+3}$ described in [7,58] (for comparison of the structures see Table 6). For τ_{13} we first considered the $SmRh_5Ge_3$-type [63] as possible structure type, but although Rietveld refinement results in a reliable R_F it reveals extremely short interatomic distances $d_{Ce1-Rh1}$=0.224 nm, $d_{Rh7-Rh1}$=0.141 nm and was therefore rejected. Analysis of the structure $U_6Co_{30}Si_{19}$ reveals an empty channel at x=y=0 with diameter 0.18781 nm for $U_6Co_{30}Si_{19}$ and 0.23296 nm for an isotypic atom

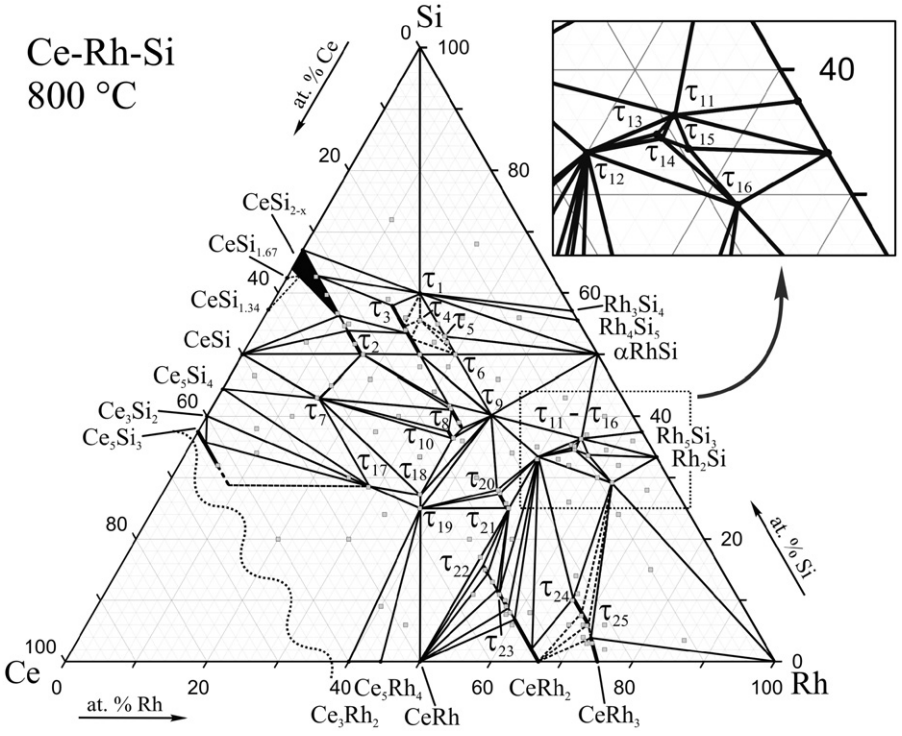

Fig. 1. Isothermal section of the ternary system Ce–Rh–Si at 800 °C. Gray squares indicates sample locations.

Table 2
Crystallographic data for phases τ_8—$Ce_2Rh_{3-x}Si_{3+x}$ (x=0.27), τ_{10}—$Ce_3Rh_{4-x}Si_{4+x}$ (x=0) and τ_{11}—$CeRh_6Si_4$ (X-ray powder diffraction at room temperature, image plate, Cu$K\alpha_1$ radiation, $20 \le 2\theta \le 100^\circ$).

Parameter/compound	τ_8—$Ce_2Rh_{3-x}Si_{3+x}$	τ_{10}—$Ce_3Rh_4Si_4$	τ_{11}—$CeRh_6Si_4$
Composition, EPMA (at%)	$Ce_{25.1}Rh_{34.2}Si_{40.6}$	$Ce_{27.1}Rh_{36.2}Si_{36.6}$	$Ce_{9.0}Rh_{54.7}Si_{36.3}$
Composition from refinement (at%)	$Ce_{25.9}Rh_{34.1}Si_{40.9}$	$Ce_{27.2}Rh_{36.4}Si_{36.4}$	$Ce_{9.1}Rh_{54.5}Si_{36.4}$
Formula from refinement	$Ce_2Rh_{2.73}Si_{3.27}$	$Ce_3Rh_4Si_4$	$CeRh_6Si_4$
Space group	*Pmmn* (No. 59)	*Immm* (No. 71)	$P\bar{6}m2$ (No. 187)
Pearson symbol	*oP*16	*oP22*	*hP*11
Prototype	$Ce_2Rh_{1.35}Ge_{4.65}$	$U_3Ni_4Si_4$	$LiCo_6P_4$
Lattice parameter (nm)	a=0.41103(1)	a=0.40676(1)	a=0.69851(1)
(Ge standard)	b=0.41047(1)	b=0.41405(1)	
	c=1.72595(2)	c=2.44689(5)	c=0.37823(1)
Reflections measured	227	173	56
Number of variables	27	26	22
$R_F=\Sigma\|F_o-F_c\|/\Sigma\|F_o\|$	0.040	0.048	0.027
$R_I=\Sigma\|I_o-I_c\|/\Sigma\|I_o\|$	0.057	0.061	0.026
$R_{wP}=[\Sigma w_i\|y_{oi}-y_{ci}\|^2/\Sigma w_i\|y_{oi}\|^2]^{1/2}$	0.046	0.040	0.033
$R_P=\Sigma\|y_{oi}-y_{ci}\|/\Sigma\|y_{0i}\|$	0.033	0.027	0.025
$R_e=[(N-P+C)/\Sigma w_i y_{oi}^2)]^{1/2}$	0.020	0.017	0.015
$\chi^2=(R_{wP}/R_e)^2$	5.4	5.5	5.1
Atom parameters			
Atom site 1	**2 Ce1** in 2*b* (1/4,3/4,*z*); *z*=0.8469(2)	**2 Ce1** in 2*a* (0,0,0)	**1 Ce1** in 1*a* (0,0,0)
occ.	1.00(−)	1.00(−)	1.00(−)
B_{iso} (10^2 nm^2)	1.64(4)	1.59(7)	0.92(2)
Atom site 2	**2 Ce2** in 2*a* (1/4,1/4,*z*); *z*=0.6458(3)	**4 Ce2** in 4*j* (1/2,0,*z*); *z*=0.3543(1)	**3 Rh1** in 3*k* (*x*,−*x*, 1/2); *x*=0.1998(1)
Occ.	1.00(−)	1.00(−)	1.00(−)
B_{iso} (10^2 nm^2)	1.64(4)	0.75(4)	0.57(3)
Atom site 3	**2 Rh1** in 2*b* (1/4,3/4,*z*); *z*=0.5022(4)	**4 Rh1** in 4*j* (1/2,0,*z*); *z*=0.0997(1)	**3 Rh2** in 3*j* (*x*,−*x*,0); *x*=0.5330(1)
Occ.	1.00(−)	1.00(−)	1.00(−)
B_{iso} (10^2 nm^2)	0.86(4)	1.19(6)	1.01(1)
Atom site 4	**2 Rh2** in 2*a* (1/4,1/4,*z*); *z*=0.0010(4)	**4 Rh2** in 4*i* (0,0,*z*); *z*=0.2499(1)	**3 Si1** in 3*k* (*x*,−*x*, 1/2); *x*=0.7984(3)
Occ.	1.00(−)	1.00(−)	1.00(−)
B_{iso} (10^2 nm^2)	0.86(4)	0.81(5)	1.49(1)
Atom site 5	**2 Si1** in 2*b* (1/4,3/4,*z*); *z*=0.0879(6)	**4 Si1** in 4*j* (1/2,0,*z*); *z*=0.1966(2)	**1 Si1** in 1*c* (1/3,2/3,0)
Occ.	1.00(−)	1.00(−)	1.00(−)
B_{iso} (10^2 nm^2)	0.86(4)	0.5(1)	1.49(1)
Atom site 6	**2 Si2** in 2*a* (1/4,1/4,*z*); *z*=0.4292(6)	**4 Si2** in 4*i* (0,0,*z*); *z*=0.4589(3)	
Occ.	1.00(−)	1.00(−)	
B_{iso} (10^2 nm^2)	0.86(4)	1.6(1)	
Atom site 7	**2 M1** in 2*b* (1/4,3/4,*z*); *z*=0.2062(4)		
Occ.	Si 0.65(2)+Rh 0.35		
B_{iso} (10^2 nm^2)	0.86(4)		
Atom site 8	**2 M2** in 2*a* (1/4,1/4,*z*); *z*=0.2798(5)		
Occ.	Si 0.62(2)+Rh 0.38		
B_{iso} (10^2 nm^2)	0.86(4)		

arrangement '$Ce_6Rh_{30}Si_{19}$' (see Fig. 3a). In case of τ_{13} the channel is broad enough to provide space for an additional atom. A difference Fourier calculation for '$Ce_6Rh_{30}Si_{19}$' in a partial *y*,*z*-section at x=0 (Fig. 3b) revealed an electron density ~75 e/Å^3 at the Wyckoff position 2*b* (0,0,0) and (0,0,1/2). Rietveld refinement for τ_{13} with an additional Si atom in the (0,0,0) position yielded an occupancy of 0.3(1) and R_F=0.042 (Table 3). The corresponding composition $Ce_6Rh_{30}Si_{19.3}$ is in good agreement with the EPMA value (Table 3).

The ternary compound τ_{20}, reported as stoichiometric $CeRh_2Si$ [10] with the fully ordered and inverse orthorhombic $CeNiSi_2$-type structure, unambiguously was detected at 800 °C at a slightly non-stoichiometric composition $CeRh_{1.88}Si_{1.12}$ (Fig. 2e). However, at the stoichiometric composition 1:2:1 we detected a new tetragonal structure (τ_{21}) isotypic to $CeIr_2Si$ [64], which coexists in equilibrium with τ_{12}—$CeRh_3Si_2$ and τ_{23}—$Ce(Rh_{1-x}Si_x)_2$ (Fig. 2f) and has a small homogeneity range $CeRh_{2-x}Si_{1+x}$ $0.0 \le x \le 0.1$. A two-phase region between τ_{20} and τ_{21} was neither detected by EPMA nor from XPD analysis.

4.1.2. *Single crystal structure determination of τ_3—$CeRh_{1-x}Si_{2+x}$ and τ_6—$Ce_2Rh_3Si_5$*

Though the crystal structures of compounds $CeRhSi_2$ and $Ce_2Rh_3Si_5$ are known, neither single crystal nor powder data are available in literature.

A single crystal, broken from as-cast alloy with nominal composition $Ce_{20}Rh_{27}Si_{53}$ revealed orthorhombic symmetry with space group *Ibam* and lattice parameters: a=0.99118(2),

Table 3
Crystallographic data for τ_{13}—$Ce_6Rh_{30}Si_{19.3}$ (X-ray powder diffraction at room temperature, image plate, Cu$K\alpha_1$ radiation, $20 \le 2\theta \le 100^\circ$).

Parameter/compound	**τ_{13}—$Ce_6Rh_{30}Si_{19.3}$**		
Composition, EPMA (at%)	$Ce_{10.7}Rh_{54.0}Si_{35.3}$		
Composition from refinement (at%)	$Ce_{10.8}Rh_{54.2}Si_{34.9}$		
Formula from refinement	$Ce_6Rh_{30}Si_{19.3}$		
Space group	$P6_3/m$ (no. 176)		
Pearson symbol	$hP110$		
Prototype	$U_6Co_{30}Si_{19}$		
Lattice parameter (nm)	a=2.2300(1)		
(Ge standard)	c=0.38398(1)		
Reflections measured	728		
Number of variables	68		
$R_F=\Sigma\lvert F_o-F_c\rvert/\Sigma\lvert F_o\rvert$	0.042		
$R_I=\Sigma\lvert I_o-I_c\rvert/\Sigma\lvert I_o\rvert$	0.057		
$R_{wP}=[\Sigma w_i\lvert y_{oi}-y_{ci}\rvert^2/\Sigma w_i\lvert y_{oi}\rvert^2]^{1/2}$	0.068		
$R_P=\Sigma\lvert y_{oi}-y_{ci}\rvert/\Sigma\lvert y_{0i}\rvert$	0.053		
$R_e=[(N-P+C)/\Sigma w_i y_{0i}^2)]^{1/2}$	0.032		
$\chi^2=(R_{wP}/R_e)^2$	4.6		
Atom parameters			
Atom sites	**1 /8/ 15 6 Ce1** in 6*h* (*x*,*y*,1/4);	**6 Rh6** in 6*h* (*x*,*y*,1/4);	**6 Si3** in 6*h* (*x*,*y*,1/4);
	x=0.5238(5)	x=0.2027(6)	x=0.124(2)
	y=0.1351(5)	y=0.0536(6)	y=0.388(2)
Occ.	1.00(−)	1.00(−)	1.00(−)
B_{iso} (10^2 nm^2)	0.42(2)	0.58(4)[a]	0.58(4)[a]
Atom sites	**2 /9/ 16 6 Ce2** in 6*h* (*x*,*y*,1/4);	**6 Rh7** in 6*h* (*x*,*y*,1/4);	**6 Si4** in 6*h* (*x*,*y*,1/4);
	x=0.2640(4)	x=0.0454(6)	x=0.761(2)
	y=0.2297(5)	y=0.4914(5)	y=0.686(2)
Occ.	1.00(−)	1.00(−)	1.00(−)
B_{iso} (10^2 nm^2)	1.44(2)	0.58(4)[a]	0.58(4)[a]
Atom sites	**3 /10/ 17 6 Rh1** in 6*h* (*x*,*y*,1/4);	**6 Rh8** in 6*h* (*x*,*y*,1/4);	**6 Si5** in 6*h* (*x*,*y*,1/4);
	x=0.5486(5)	x=0.0064(5)	x=0.069(2)
	y=0.3055(6)	y=0.3579(6)	y=0.184(2)
Occ.	1.00(−)	1.00(−)	1.00(−)
B_{iso} (10^2 nm^2)	0.58(4)[a]	0.58(4)[a]	0.58(4)[a]
Atom sites	**4 /11/ 18 6 Rh2** in 6*h* (*x*,*y*,1/4);	**6 Rh9** in 6*h* (*x*,*y*,1/4);	**6 Si6** in 6*h* (*x*,*y*,1/4);
	x=0.8008(5)	x=0.3559(6)	x=0.006(2)
	y=0.2051(5)	y=0.6095(6)	y=0.579(2)
Occ.	1.00(−)	1.00(−)	1.00(−)
B_{iso} (10^2 nm^2)	0.58(4)[a]	0.58(4)[a]	0.58(4)[a]
Atom sites	**5 /12/ 19 6 Rh3** in 6*h* (*x*,*y*,1/4);	**6 Rh10** in 6*h* (*x*,*y*,1/4);	**2 Si7** in 2*d* (2/3,1/3,1/4)
	x=0.6573(6)	x=0.1048(5)	
	y=0.1040(5)	y=0.0960(5)	
Occ.	1.00(−)	1.00(−)	1.00(−)
B_{iso} (10^2 nm^2)	0.58(4)[a]	0.58(4)[a]	0.58(4)[a]
Atom sites	**6 /13/ 20 6 Rh4** in 6*h* (*x*,*y*,1/4);	**6 Si1** in 6*h* (*x*,*y*,1/4);	**2 Si8** in 2*b* (0,0,0)
	x=0.2891(7)	x=0.471(2)	
	y=0.3917(6)	y=0.632(2)	
Occ.	1.00(−)	1.00(−)	0.3 (1)
B_{iso} (10^2 nm^2)	0.58(4)[a]	0.58(4)[a]	0.58(4)[a]
Atom sites	**7/14 6 Rh5** in 6*h* (*x*,*y*,1/4);	**6 Si2** in 6*h* (*x*,*y*,1/4);	
	x=0.1611(6)	x=0.239(2)	
	y=0.3004(5)	y=0.470(2)	
Occ.	1.00(−)	1.00(−)	
B_{iso} (10^2 nm^2)	0.58(4)[a]	0.58(4)[a]	

[a] Constrained parameters.

b=1.17558(3), c=0.58313(1) nm. Direct methods yielded a completely ordered atom arrangement isotypic with the structure type of $U_2Co_3Si_5$. Results of the refinement for $Ce_2Rh_3Si_5$, which converged to $R_F = 0.026$ are summarized in Table 7.

The X-ray diffraction pattern of a single crystal from the as-cast sample $Ce_{25}Rh_{16}Si_{59}$ was indexed with orthorhombic symmetry: space group *Cmcm* and lattice parameters a=0.42604(2), b=1.67737(6), c=0.41787(1) nm. The structure type $CeNiSi_2$ for τ_3 was confirmed by X-ray single crystal refinement. Atom parameters and results of the refinement for $CeRh_{0.76}Si_{2.24}$, which converged to $R_F = 0.017$ with residual electron densities smaller than $\pm 3.2\,e^-/Å^3$, are summarized in Table 6.

4.2. Phase relations and isothermal section of the Ce–Rh–Si system at 800 °C

Table 8 summarizes compositions, structure type and lattice parameters for all the phases involved in three-phase equilibria at 800 °C. Besides the ternary compounds mentioned in Sections

Table 4
Crystallographic data for phases τ_{17}—$Ce_3Rh_2Si_2$, τ_{18}—$Ce_4Rh_4Si_3$ and τ_{22}—$Ce_2Rh_{3+x}Si_{1-x}$ (x=0.15) (X-ray powder diffraction at room temperature, image plate, Cu$K\alpha_1$ radiation, $20 \le 2\theta \le 100^\circ$).

Parameter/compound	τ_{17}—$Ce_3Rh_2Si_2$	τ_{18}—$Ce_4Rh_4Si_3$	τ_{22}—$Ce_2Rh_{3+x}Si_{1-x}$
Composition, EPMA (at%)	$Ce_{42.6}Rh_{28.5}Si_{29.0}$	$Ce_{36.4}Rh_{36.6}Si_{27.0}$	$Ce_{33.2}Rh_{52.0}Si_{14.8}$
Composition from refinement (at%)	$Ce_{42.8}Rh_{28.6}Si_{28.6}$	$Ce_{36.4}Rh_{36.4}Si_{27.2}$	$Ce_{33.3}Rh_{52.4}Si_{14.3}$
Formula from refinement	$Ce_3Rh_2Si_2$	$Ce_4Rh_4Si_3$	$Ce_2Rh_{3.15}Si_{0.85}$
Space group	*Pbcm* (No. 57)	*C*2/*c* (No. 15)	$R\bar{3}m$ (No. 166)
Pearson symbol	*oP*28	*mC*44	*hR*18
Prototype	$La_3Ni_2Ga_2$	$Sm_4Pd_4Si_3$	Y_2Rh_3Ge
Lattice parameter (nm)	a=0.56910(1)	a=2.07512 (4)	a=0.55495(1)
(Ge standard)	b=0.79829(1)	b=0.57208 (1)	
	c=1.32895(2)	c=0.78776 (1)	c=1.18616(1)
		β=110.11(1)°	
Reflections measured	370	553	59
Number of variables	31	38	21
$R_F=\Sigma\|F_o-F_c\|/\Sigma\|F_o\|$	0.051	0.026	0.047
$R_I=\Sigma\|I_o-I_c\|/\Sigma\|I_o\|$	0.062	0.031	0.051
$R_{wP}=[\Sigma w_i\|y_{oi}-y_{ci}\|^2/\Sigma w_i\|y_{oi}\|^2]^{1/2}$	0.034	0.013	0.036
$R_P=\Sigma\|y_{oi}-y_{ci}\|/\Sigma\|y_{oi}\|$	0.025	0.010	0.027
$R_e=[(N-P+C)/\Sigma w_i y_{oi}^2)]^{1/2}$	0.018	0.009	0.015
$\chi^2=(R_{wP}/R_e)^2$	3.6	2.3	5.9
Atom parameters			
Atom site 1	**8 Ce1** in 8*e* (*x*,*y*,*z*);	**8 Ce1** in 8*f* (*x*,*y*,*z*);	**6 Ce1** in 6*c* (0,0,*z*);
	x=0.1403(2)	x=0.0656(1)	z=0.3758(1)
	y=0.3913(1)	y=0.1350(2)	
	z=0.1002(1)	z=0.6701(1)	
Occ.	1.00(−)	1.00(−)	1.00(−)
B_{iso} (10^2 nm^2)	1.53(3)	1.13(3)	0.78(2)
Atom site 2	**4 Ce2** in 4*d* (*x*,*y*,1/4);	**8 Ce2** in 8*f* (*x*,*y*,*z*);	**9 Rh1** in 9*d* (1/2,0,1/2)
	x=0.6418(3)	x=0.3296(1)	
	y=0.2449(2)	y=0.8828(2)	
		z=0.0980(1)	
Occ.	1.00(−)	1.00(−)	1.00(−)
B_{iso} (10^2 nm^2)	0.55(4)	0.41(3)	1.03(2)
Atom site 3	**8 Rh1** in 8*e* (*x*,*y*,*z*);	**8 Rh1** in 8*f* (*x*,*y*,*z*);	**3 M** in 3*a* (0,0,0)
	x=0.3773(4)	x=0.0606(1)	
	y=0.0347(1)	y=0.3635(3)	
	z=0.0921(1)	z=0.0189(2)	
Occ.	1.00(−)	1.00(−)	0.86(1) Si+0.14 Rh
B_{iso} (10^2 nm^2)	2.07(4)	1.51(4)	0.5(1)
Atom site 4	**4 Si1** in 4*d* (*x*,*y*,1/4);	**8 Rh2** in 8*f* (*x*,*y*,*z*);	
	x=0.140(1)	x=0.2212(1)	
	y=0.1033(7)	y=0.1474(3)	
		z=0.8203(2)	
Occ.	1.00(−)	1.00(−)	
B_{iso} (10^2 nm^2)	1.3(2)	1.56(4)	
Atom site 5	**4 Si1** in 4*c* (*x*,1/4,0);	**4 Si1** in 4*e* (0,*y*, 1/4);	
	x=0.640(1)	y=0.359(1)	
Occ.	1.00(−)	1.00(−)	
B_{iso} (10^2 nm^2)	2.9(2)	0.5(1)	
Atom site 6		**8 Si2** in 8*f* (*x*,*y*,*z*);	
		x=0.1763(2)	
		y=0.8716(9)	
		z=0.5743(7)	
Occ.		1.00(−)	
B_{iso} (10^2 nm^2)		0.37(9)	

4.1.1 and 4.1.2, we detected a ternary phase (τ_{23}) with unknown structure and composition range $Ce_{33.3}Rh_{58.2-55.2}Si_{8.5-11.5}$. The major reflections of the XPD pattern of τ_{23} may be indexed on the basis of an orthorhombic structure with $a_0 \approx 0.51$ nm, $b_0 \approx 0.55$ nm and $c_0 \approx 0.75$ nm, which suggests isotypism with the orthorhombic low-temperature modification of UMn_2 [65]. However, full profile analysis for this structure model did not result in a satisfactory description of the observed intensities. As the X-ray diffraction pattern reveals additional reflections, several samples with 33 at% of Ce were prepared. X-ray reflections of the phase in ternary samples with 10, 11 and 13 at% of Si were fully indexed on a supercell $a=3a_0$, $b=b_0$, $c=c_0$, unlike the superstructure reflections of the phase in samples with 8 and 9 at% of Si. As the correct crystal structure is unavailable we are presently unable to decide whether the composition range of τ_{23} contains one or two phases.

Consistent with an incongruent formation of τ_{18}—$Ce_4Rh_4Si_3$ ($Sm_4Pd_4Si_3$-type, see Table 2) from the melt, an as-cast sample $Ce_{36.5}Rh_{36.5}Si_{27}$ (composition close to $Ce_4Rh_4Si_3$) shows primary grains of τ_9 surrounded by secondary crystals of τ_8 whilst τ_{18} and binary Ce_5Rh_4 crystallize from the last portion of the liquid (see Fig. 2g). It is interesting to note, that ternary τ_{19} and τ_{10}, which both lie close to the described crystallization line, are not observed in the as-cast alloy, and τ_{10} appears only after anneal of

Table 5
Crystallographic data for τ_{24}—$Ce_8(Rh_{1-x}Si_x)_{24}Si$ and τ_{25}—$Ce_4(Rh_{1-x}Si_x)_{12}Si$ (X-ray powder diffraction at room temperature, image plate, Cu$K\alpha_1$ radiation, $20 \le 2\theta \le 100^\circ$).

Parameter/compound	**τ_{24}—$Ce_8(Rh_{1-x}Si_x)_{24}Si$**	**τ_{25}—$Ce_4(Rh_{1-x}Si_x)_{12}Si$**
Composition, EPMA (at%)	$Ce_{23.5}Rh_{66.5}Si_{10}$	$Ce_{23.5}Rh_{70.5}Si_6$
Composition from refinement (at%)	$Ce_{24.2}Rh_{66.4}Si_{9.6}$	$Ce_{23.5}Rh_{70.6}Si_{5.9}$
Formula from refinement	$Ce_8Rh_{21.9}Si_{3.1}$	$Ce_4Rh_{12}Si$
Space group	$Pm\bar{3}m$ (No 221)	$Im\bar{3}m$ (No 229)
Pearson symbol	$cP33$	$cI34$
Prototype	$Ce_8Pd_{24}Sb$	$Ce_4Rh_{12}Si$
Lattice parameter (nm) (Ge standard)	a=0.82501(1)	a=0.82154(1)
Reflections measured	100	43
Number of variables	19	18
$R_F=\Sigma\lvert F_o-F_c\rvert/\Sigma\lvert F_o\rvert$	0.059	0.035
$R_I=\Sigma\lvert I_o-I_c\rvert/\Sigma\lvert I_o\rvert$	0.048	0.029
$R_{wP}=[\Sigma w_i\lvert y_{oi}-y_{ci}\rvert^2/\Sigma w_i\lvert y_{oi}\rvert^2]^{1/2}$	0.026	0.029
$R_P=\Sigma\lvert y_{oi}-y_{ci}\rvert/\Sigma\lvert y_{0i}\rvert$	0.019	0.021
$R_e=[(N-P+C)/\Sigma w_i y_{oi}^2)]^{1/2}$	0.014	0.014
$\chi^2=(R_{wP}/R_e)^2$	3.4	4.2
Atom parameters		
Atom site 1	**8 Ce1** in 8*g* (*x*,*x*,*x*); *x*=0.2483(1)	**8 Ce1** in 8*c* (1/4,1/4,1/4)
Occ.	1.00(−)	1.00(−)
B_{iso} (10^2 nm^2)	0.78(2)	0.30(2)
Atom site 2	**12 Rh1** in 12*h* (*x*,1/2,0); *x*=0.2464(2)	**12 Rh1** in 12*d* (1/4,0,1/2)
Occ.	1.00(−)	1.00(−)
B_{iso} (10^2 nm^2)	0.93(2)	0.91(3)
Atom site 3	**6 M** in 6*e* (*x*,0,0); *x*=0.2940(2)	**12 Rh2** in 12*e* (*x*,0,0); *x*=0.2729(1)
Occ.	0.64(1) Rh+0.36 Si	1.00(−)
B_{iso} (10^2 nm^2)	1.71(6)	1.80(4)
Atom site 4	**6 Rh2** in 6*f* (*x*, 1/2,1/2); *x*=0.2345(2)	**2 Si1** in 2*a* (0,0,0);
Occ.	1.00(−)	1.00(−)
B_{iso} (10^2 nm^2)	2.18(3)	1.5(2)
Atom site 5	**1 Si1** in 1*a* (0,0,0)	
Occ.	1.00(−)	
B_{iso} (10^2 nm^2)	1.7(2)	

this sample at 800 °C (Fig. 2h). Such a behavior indicates that τ_{10} does not form from the liquid but rather forms from a solid-state reaction.

The strong increase of the cell parameters for the ternary homogeneity region of $CeRh_3$ dissolving Si (Table 1) suggests an interstitial incorporation of Si atoms in the crystal structure. For alloy $Ce_{24}Rh_{73}Si_3$ Rietveld refinement of the $CeRh_3$ (Cu_3Au-type) structure with statistical occupation of Si in position (1/2,1/2,1/2) resulted in a slightly lower residual value R_F=0.034 ($CeRh_3Si_{1-x}$) than for Si/Rh substitution in the (0,1/2,1/2) position ($Ce(Rh,Si)_3$, R_F=0.036). With increasing Si content EPMA revealed a constant Ce concentration for the composition region $Ce_{23.5}Rh_{70.5-66.5}Si_{6-10}$ (23.5 ± 0.5 at%). The X-ray diffraction pattern for the alloy $Ce_{23.5}Rh_{66.5}Si_{10}$ was found to be very similar to $CeRh_3Si_{1-x}$, but additional reflections indicated a two-fold superstructure ($a \sim 2a_{CeRh3}$). Whereas the XPD pattern of the sample with composition $Ce_{23.5}Rh_{69}Si_{7.5}$ shows the two-fold supercell reflections but with systematic extinctions $h+k+l=2n+1$ for a *bcc* structure, the XPD pattern of $Ce_{23.5}Rh_{66.5}Si_{10}$ reveals a cubic primitive two-fold superstructure. For a comparison of both patterns see Fig. 4. A structural model according to $Ce_8Pd_{24}Sb$ (SG $Pm\bar{3}m$) as proposed by Gordon and DiSalvo [66] was successfully employed to refine the primitive XPD pattern of $Ce_{23.5}Rh_{66.5}Si_{10}$ (results are presented in Table 2, R_F=0.059, $d_{Si1-Rh2}$=0.2417 nm). Consequently, Rietveld refinement for the *bcc* structure (at lower Si-contents) was based on the $Ce_8Pd_{24}Sb$-type model ($Ce_8Rh_{24}Si_{1-x}$) with an additional Si-atom in (1/2,1/2,1/2) yielding R_F=0.035 (Table 2, $d_{Si1-Rh2}$=0.2242 nm). For comparison of these structures with $CeRh_3$ see Fig. 5. In accordance to the existence of these two phases, the $Ce_{23.5}Rh_{70.5-66.5}Si_{6-10}$ region was split into two parts: τ_{24}—$Ce_8(Rh_{1-x}Si_x)_{24}Si$ ($0.07 \le x \le 0.10$) and τ_{25}—$Ce_4(Rh_{1-x}Si_x)_{12}Si$ ($0.0 \le x \le 0.03$), though a two-phase region was not detected by means of EPMA and XPD. It should be noted, that although there is a constant increase of cell parameters within the composition range $Ce_{23.5}Rh_{70.5-66.5}Si_{6-10}$, the structure of τ_{25}—$Ce_4(Rh_{1-x}Si_x)_{12}Si$ exhibits a Si atom in (1/2,1/2,1/2), whereas this site is vacant in Si-rich τ_{24}. However, Rietveld refinement for τ_{24} with a Si2 atom in (1/2,1/2,1/2) resulted in a worse R_F=0.07 and a very short distance $d_{Si2-Rh2}$=0.2176 nm. It should be furthermore mentioned, that in all XPD patterns of $CeRh_3Si_{1-x}$, τ_{24} and τ_{25}, two still unindexed reflections appear at $2\theta \approx 12.2^\circ$ and 14.1° (Fig. 4) with an intensity comparable to the (1 1 0) reflection and that the 2θ values of these reflections follow the changes in Si concentration. τ_{24} forms directly from the liquid and at 800 °C this phase is in equilibrium with τ_{12} and $CeRh_2$ (Fig. 2i and j).

A new phase τ_5—$Ce_{20}Rh_{27}Si_{53}$ was detected between the compounds τ_1—$CeRhSi_3$ and τ_6—$Ce_2Rh_3Si_5$. The X-ray pattern of this phase looks very similar to τ_1 and reflections can be indexed on a tetragonal cell with parameters a=0.41391(1) nm, c=0.99650(2) nm, which lie between the parameters of τ_1 ($BaNiSn_3$-type as an ordered variant of $BaAl_4$-type; a=0.42311 (1) nm, c=0.97816(3) nm) and τ_9—$CeRh_2Si_2$ ($ThCr_2Si_2$-type as another ordered variant of $BaAl_4$-type; a=0.40883(1) nm,

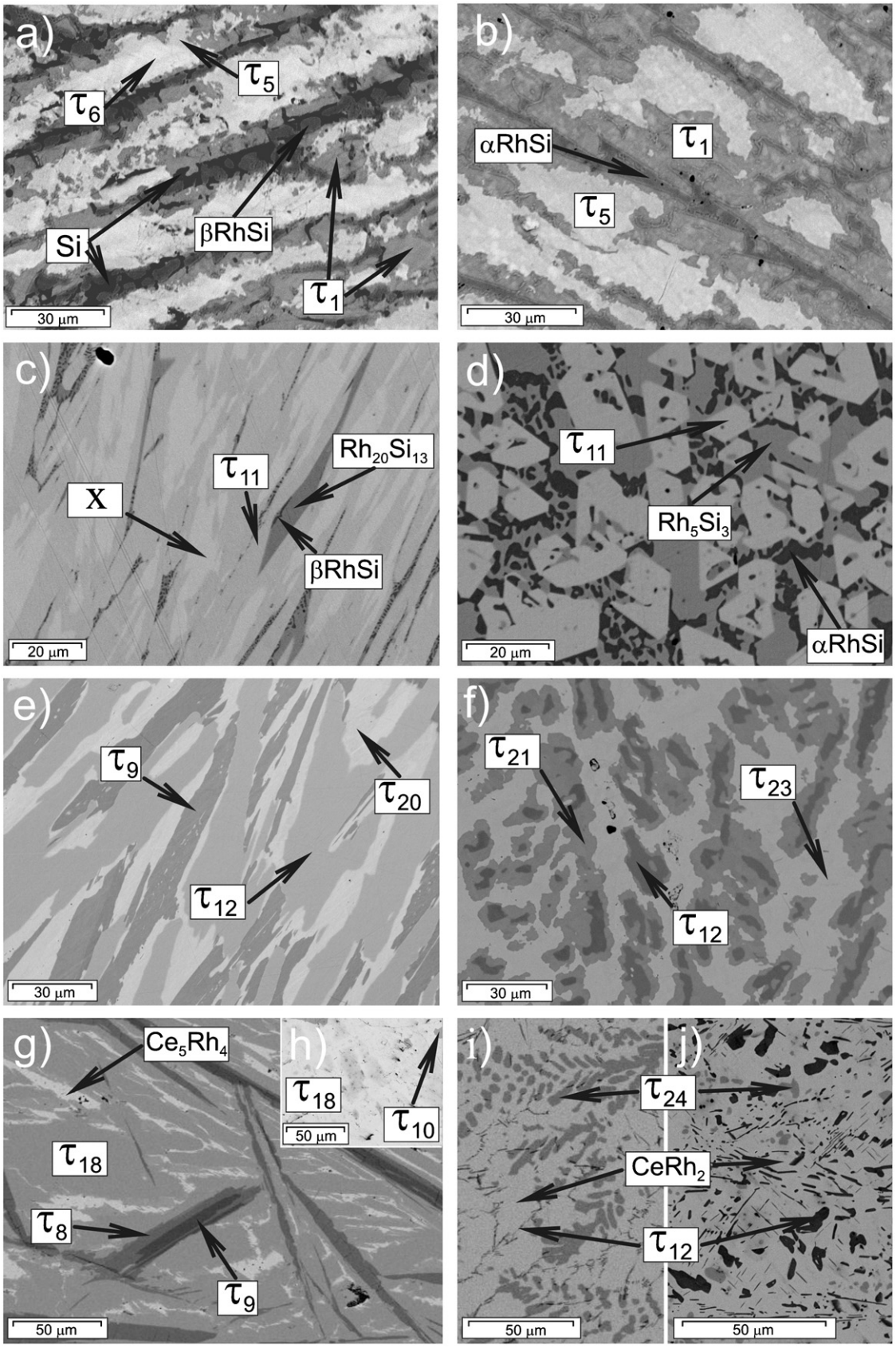

Fig. 2. Microstructure of selected Ce–Rh–Si alloys: $Ce_{16}Rh_{28}Si_{56}$ ((a) as-cast; (b) 800 °C), $Ce_8Rh_{55}Si_{37}$ ((c) as-cast, X—$Ce_{10.5}Rh_{54.4}Si_{35.1}$), $Ce_4Rh_{56}Si_{40}$ ((d) 800 °C), $Ce_{20}Rh_{46}Si_{34}$ ((e) 800 °C), $Ce_{27}Rh_{53}Si_{20}$ ((f) 800 °C), $Ce_{36.5}Rh_{36.5}Si_{27}$ ((g) as-cast; (h) 800 °C), $Ce_{30}Rh_{62}Si_8$ ((i) as-cast; (j) 800 °C).

Table 6
Hexagonal structures with $c \approx 0.38$ nm, which belong to the structure series with general formula $Ce_{n(n+1)}Rh_{6(n^2+1)}Si_{4n^2+3}$.

N	Compound	Structure type	Pearson symbol	Cell parameters (nm)		Crystal chemical formula
				a	c	
∞	τ_{11}—$CeRh_6Si_4$	$LiCo_6P_4$	*hP*11	0.69881(2)	0.37808(2)	$CeRh_6Si_4$
1	τ_{15}—$Ce_2Rh_{12}Si_7$	$Ho_2Rh_{12}As_7$	*hP*24-3	0.97199(2)	0.38480(1)	$Ce_2Rh_{12}Si_7$
2	τ_{14}—$Ce_6Rh_{30}Si_{19}$	$Sc_6Co_{30}Si_{19}$	*hP*62-7	1.57257(2)	0.38569(1)	$Ce_6Rh_{30}Si_{19}$
3	τ_{13}—$Ce_6Rh_{30}Si_{19.3}$	$U_6Co_{30}Si_{19}$	*hP*110	2.2300(1)	0.38398(1)	$Ce_{12}Rh_{60}Si_{38.6}$
4	τ_{25}—$Ce_{10}Rh_{51}Si_{33}$	$U_{10}Co_{51}Si_{33}$	*hP*188	2.9107(1)	0.38334(1)	$Ce_{20}Rh_{102}Si_{66}$

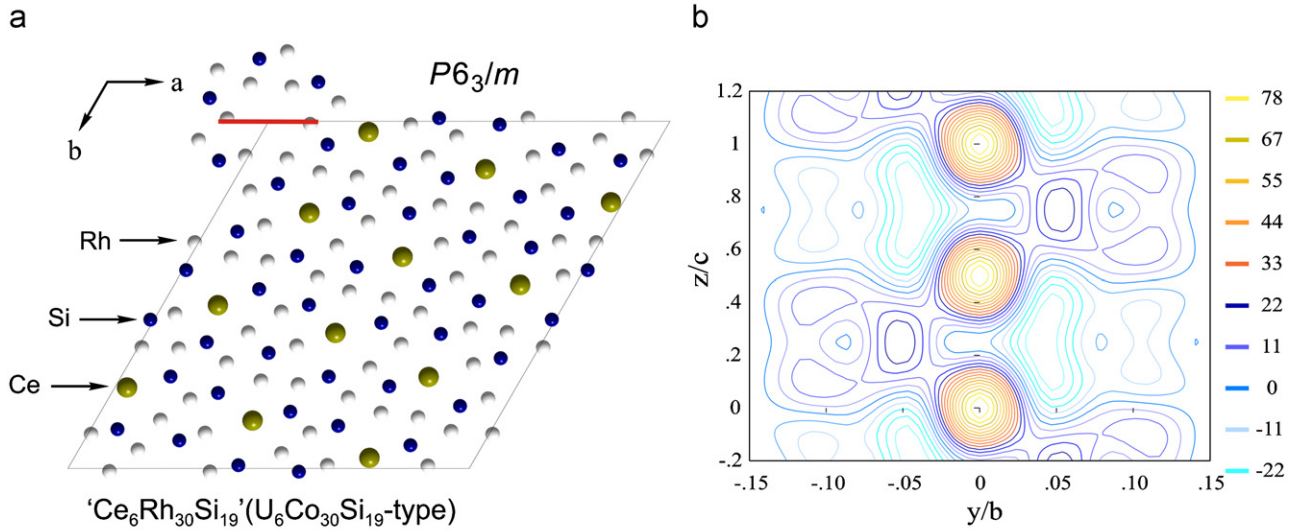

Fig. 3. Crystal structure of '$Ce_6Rh_{30}Si_{19}$' ($U_6Co_{30}Si_{19}$-type) with empty channels at $x=y=0$ (a). Difference Fourier map for the structure along the partial section $x=0$; $-0.15 \le y \le 0.15$; $-0.2 \le z \le 1.2$ (marked by a thick solid line) (b).

$c=1.01748(2)$ nm). Nevertheless the presence of additional reflections presently does not allow a structure designation for τ_5. The phases τ_1 and τ_5 are, however, clearly distinguishable by BSD contrast (see Fig. 2a and b) and have a distinct grain boundary. The significant difference in the lattice parameters for these phases results in well separated X-ray patterns. In order to exclude the possibility that two different compositions are observed due to phase-segregation during crystallization from the liquid, the two-phase alloy $Ce_{20}Rh_{25}Si_{55}$ ($\tau_1+\tau_5$) was subjected to heat treatment at 800 °C under various conditions: (a) anneal of the bulk as-cast alloy for 14 days, (b) sample was powdered to grain size below 20 μm, cold compacted and sintered for 7 days, (c) powders were hot pressed at 800 °C for 2 h and annealed for 3 days. After all these treatments, the lattice parameters for τ_1 and τ_5 do not show any change that may indicate a single-phase region for these phases at 800 °C. Furthermore, the phases τ_1, τ_5 and binary RhSi form a ternary equilibrium at 800 °C (Fig. 2b).

The annealing temperature of 800 °C was chosen in order to achieve enhanced diffusion in the system combining elements with rather different melting points. In general this temperature was enough for reaching equilibrium (see Fig. 2), but in some cases additional heat treatment was required. Thus more than three phases were detected by EPMA and XPD analysis for some samples after annealing at 800 °C for 1 month. Particularly it concerns equilibria involving τ_8 and τ_{10} phases. In these cases samples were powdered, cold pressed and annealed at 800 °C for 4 days. Equilibria for these regions were established from comparison of XPD patterns of the samples in different states. Phase analysis of the samples prepared in the region of τ_4 (dashed lines) encountered similar problems, but due to unknown structure of the phase, solid evidence of phase equilibria cannot be presented. Moreover, EPMA of τ_4 shows a 2 at% spread of values of composition.

4.2.1. High- and low-temperature phases

The ternary compound τ_{26}—$Ce_{10}Rh_{51}Si_{33}$ was detected by means of XPD phase analysis in the as-cast alloy $Ce_{10.7}Rh_{53.7}Si_{35.6}$ together with τ_{11}, τ_{12} and τ_{13}. However, a sample prepared at the stoichiometric composition $Ce_{10}Rh_{51}Si_{33}$ (=$Ce_{10.6}Rh_{53.3}Si_{35.1}$) neither contains the τ_{26} phase in as-cast nor in annealed states. We observed τ_{13} as a major phase with small amounts of τ_{11} and τ_{12} (and with Rh_2Si in the as-cast alloy). Because of the fact that during equilibration of the cast alloy $Ce_{10.7}Rh_{53.7}Si_{35.6}$ at 800 °C the amount of τ_{26}—$Ce_{10}Rh_{51}Si_{33}$ significantly decreased and completely disappeared after annealing at 1050 °C, we consider τ_{26} to be a high temperature phase, which does not participate in the phase equilibria at 800 °C. It should be mentioned that due to the close compositions, EPMA is unable to distinguish between τ_{13} and τ_{26} phases.

Another high temperature phase—CeRhSi—was found in the as-cast sample $Ce_{33}Rh_{33}Si_{34}$ by means of EPMA analysis. The reflections of the unknown phase in the XPD pattern were indexed completely on the basis of a primitive cubic unit cell with cell parameter $a=0.6231(1)$ nm and found to belong to the LaIrSi structure type. The phase completely disappeared after annealing at 800 °C as well as at 1050 °C.

Table 7
X-ray single crystal data at RT for τ_3—$CeRh_{1-x}Si_{2+x}$ and τ_6—$Ce_2Rh_3Si_5$ (Mo$K\alpha$ radiation); structure data are standardized with program *Structure Tidy* [58].

Parameter/compound	**τ_3—$CeRh_{1-x}Si_{2+x}$**	**τ_6—$Ce_2Rh_3Si_5$**
Nominal composition	$CeRh_{0.76}Si_{2.24}$	$Ce_2Rh_3Si_5$
Crystal size (μm)	30 × 30 × 30	50 × 50 × 50
Space group	*Cmcm* (No. 63)	*Ibam* (No. 72)
Prototype	$CeNiSi_2$	$U_2Co_3Si_5$
Pearson symbol	*oS*16	*oI*40
Lattice parameters (nm)	*a*=0.42604(2) *b*=1.67737(6) *c*=0.41787(1)	*a*=0.99118(2) *b*=1.17558(3) *c*=0.58313(1)
Volume (nm^3)	0.29862(3)	0.67947(2)
μ_{abs} (mm^{-1})	21.04	21.03
2θ range up to (deg)	72.34	72.49
Reflections in refinement	$398 \geq 4\sigma(F_o)$ of 424	$829 \geq 4\sigma(F_o)$ of 863
Index range	$-6 \leq h \leq 6$ $-25 \leq k \leq 27$ $-6 \leq l \leq 6$	$-15 \leq h \leq 16$ $-19 \leq k \leq 19$ $-9 \leq l \leq 9$
Calculated density (g/cm^3)	6.66	7.13
Number of variables	19	37
$R_F=\Sigma\|F_o-F_c\|/\Sigma\|F_o\|$	0.017	0.026
R_{Int}	0.011	0.012
wR^2	0.054	0.063
GOF	1.294	1.096
Extinction	0.0024(8)	0.0039(2)
Atom parameters		
Atom site 1	**4 Ce1** in 4*c* (0,*y*,1/4); *y*=0.39488(2)	**8 Ce1** in 8*j* (*x*,*y*,0); *x*=0.26612(3) *y*=0.36895(2)
Occ.	1.00(−)	1.00(−)
U_{11},U_{22},U_{33} (in 10^2 nm^2)	0.0071(2), 0.0063(2), 0.0068(2)	0.0069(2), 0.0049(1), 0.0059(1)
U_{23},U_{13},U_{12} (in 10^2 nm^2)	0, 0, 0	0, 0, −0.0004(1)
Atom site 2	**4 M1** in 4*c* (0,*y*,1/4); *y*=0.18149(4)	**8 Rh1** in 8*j* (*x*,*y*,0); *x*=0.10789(4) *y*=0.13811(3)
Occ.	0.762(4) Rh+0.238 Si	1.00(−)
U_{11},U_{22},U_{33} (in 10^2 nm^2)	0.0072(3), 0.0075(3), 0.0058(3)	0.0061(2), 0.0053(2), 0.0086(2)
U_{23},U_{13},U_{12} (in 10^2 nm^2)	0, 0, 0	0, 0, 0.0001(1)
Atom site 3	**4 Si1** in 4*c* (0,*y*,1/4); *y*=0.0376(1)	**4 Rh2** in 4*b* (1/2,0,1/4)
Occ.	1.00(−)	1.00(−)
U_{11},U_{22},U_{33} (in 10^2 nm^2)	0.0094(9), 0.0121(9),0.0079(9)	0.0059(2), 0.0057(2), 0.0064(2)
U_{23},U_{13},U_{12} (in 10^2 nm^2)	0, 0, 0	0, 0, 0
Atom site 4	**4 Si2** in 4*c* (0,*y*,1/4); *y*=0.7493(1)	**8 Si1** in 8*j* (*x*,*y*,0); *x*=0.3469(2) *y*=0.1068(1)
Occ.	1.00(−)	1.00(−)
U_{11},U_{22},U_{33} (in 10^2 nm^2)	0.0095(8), 0.0066(7),0.0069(8)	0.0165(8), 0.0082(6), 0.0075(6)
U_{23},U_{13},U_{12} (in 10^2 nm^2)	0, 0, 0	0, 0, 0.0030(5)
Atom site 5		**8 Si2** in 8*g* (0,*y*,1/4); *y*=0.2751(1)
Occ.		1.00(−)
U_{11},U_{22},U_{33} (in 10^2 nm^2)		0.0069(6), 0.0096(6), 0.0086(5)
U_{23},U_{13},U_{12} (in 10^2 nm^2)		0, 0.0012(4), 0
Atom site 5		**4 Si3** in 4*a* (0,0,1/4);
Occ.		1.00(-)
U_{11},U_{22},U_{33} (in 10^2 nm^2)		0.0058(8), 0.0061(8), 0.0091(8)
U_{23},U_{13},U_{12} (in 10^2 nm^2)		0, 0, 0
Residual density; e/Å^3 max; min	3.13; −1.12	8.02; −2.80
Principal mean square atomic displacements of U_{ij}	Ce1 0.0070 0.0068 0.0063 M1 0.0075 0.0072 0.0058 Si1 0.0121 0.0094 0.0079 Si2 0.0095 0.0069 0.0066	Ce1 0.0070 0.0059 0.0048 Rh1 0.0086 0.0061 0.0053 Rh2 0.0064 0.0059 0.0057 Si1 0.0175 0.0075 0.0073 Si2 0.0096 0.0092 0.0062 Si3 0.0091 0.0061 0.0058

Low-temperature binary Rh_3Si_2 was not formed during phase transformation in the $Ce_4Rh_{56}Si_{40}$ alloy (see Fig. 2d) confirming data of Palenzona et al. [61] on the metastable nature of this phase. Consequently the equilibrated alloy consists of αRhSi, Rh_5Si_3 and τ_{11}—$CeRh_6Si_4$.

5. Conclusions

Phase relations in the ternary system Ce–Rh–Si have been established for the isothermal section at 800 °C based on X-ray powder and single crystal diffraction, SEM and EMPA on about 80

Table 8
Data on alloys from three-phase regions in the Ce–Pd–Si system at 800 °C.

Three-phase field	Phase	EPMA (at%)			Lattice parameters (nm)		
		Ce	Rh	Si	*a*	*b*	*c*
(Si)+$CeSi_2$+τ_1	(Si)	2.6	0.0	97.4	0.54226(3)		
	$CeSi_2$	33.2	0.0	66.8	0.42007(2)		1.3943(1)
	τ_1	19.4	20.4	60.2	0.42311(1)		0.97816(3)
(Si)+Rh_3Si_4+τ_1	(Si)	0.0	0.0	100.0	0.54246(2)		
	Rh_3Si_4	0.0	43.0	57.0	1.8800(1)	0.36048(2)	0.58089(3)
	τ_1	19.4	20.7	59.9	0.42319(1)		0.97787(4)
$CeSi_2$+τ_1+τ_3	$CeSi_2$	33.4	3.6	63.0	0.41965(9)		1.3929(5)
	τ_1	20.2	19.4	60.4	0.42327(5)		0.97837(2)
	τ_3	24.9	16.6	58.5	0.42566(4)	1.6768(2)	0.41763(4)
τ_1+τ_4+τ_5	τ_1	20.0	20.2	59.8	0.42338(2)		0.98074(6)
	τ_4	21.3	22.4	56.3	–	–	–
	τ_5	19.8	27.3	52.9	0.41424(2)		0.99663(5)
αRhSi+τ_1+τ_5	αRhSi	0.0	50.3	49.7	0.55466(5)	0.30707(2)	0.63658(5)
	τ_1	19.3	20.8	59.9	0.42309(1)		0.97835(3)
	τ_5	19.3	28.5	52.2	0.41346(1)		0.99404(5)
Rh_4Si_5+αRhSi+τ_1	Rh_4Si_5	0.0	44.3	55.7	1.23348(8)	0.35071(2)	0.59285(4)
	αRhSi	0.0	50.0	50.0	0.55467(7)	0.30773(3)	0.63583(7)
	τ_1	19.9	20.2	59.9	0.42341(1)		0.97779(5)
CeSi+$CeSi_2$+τ_2	CeSi	49.1	0.0	50.9	0.82678(7)	0.39704(3)	0.59768(4)
	$CeSi_2$	33.6	9.4	57.0	0.41789(1)		1.41310(5)
	τ_2	33.3	12.7	54.0	0.82068(1)		0.85030(2)
$CeSi_2$+τ_3+τ_2	$CeSi_2$	33.4	9.6	57.0	0.41781(1)		1.41377(2)
	τ_3	25.3	21.5	53.2	0.42618(2)	1.67475(8)	0.41747(2)
	τ_2	33.6	13.6	52.8	0.82162(1)		0.84804(2)
τ_4+τ_5+τ_6	τ_4	22.4	22.7	54.9	–	–	–
	τ_5	19.9	26.9	53.2	0.41388(1)		0.99486(5)
	τ_6	20.1	30.1	49.8	0.99003(3)	1.17412(4)	0.58187(2)
CeSi+Ce_5Si_4+τ_7	CeSi	49.0	0.0	51.0	0.82832(3)	0.39756(1)	0.59601(2)
	Ce_5Si_4	54.1	0.0	45.9	0.79482(7)		1.5143(2)
	τ_7	42.1	14.5	43.4	0.41624(3)	0.42536(3)	1.82139(2)
CeSi+τ_2+τ_7	CeSi	49.7	0.0	50.3	0.82876(9)	0.39694(4)	0.59685(7)
	τ_2	33.7	16.7	49.6	0.82359(2)		0.84212(3)
	τ_7	42.7	14.4	42.9	0.41528(1)	0.42548(1)	1.81906(5)
τ_2+τ_7+τ_8	τ_2	33.5	17.0	49.5	0.82283(2)		0.84149(3)
	τ_7	42.4	14.5	43.1	0.41483(3)	0.42493(3)	1.8176(1)
	τ_8	25.0	34.1	40.9	0.40968(3)	0.41094(3)	1.7221(1)
τ_2+τ_3+τ_8	τ_2	33.4	17.0	49.6	0.82403(2)		0.84280(3)
	τ_3	24.7	25.2	50.1	0.42629(1)	1.67456(3)	0.41731(1)
	τ_8	25.0	32.7	42.3	0.41243(2)	0.40980(1)	1.72551(7)
τ_3+τ_8+τ_9	τ_3	25.1	24.8	50.1	0.42562(3)	1.6716(1)	0.41673(3)
	τ_8	25.0	32.7	42.3	0.41167(2)	0.40920(2)	1.72339(6)
	τ_9	20.0	39.7	40.3	0.40836(1)		1.01565(3)
τ_3+τ_6+τ_9	τ_3	24.7	25.2	50.1	0.42613(1)	1.67520(5)	0.41705(1)
	τ_6	20.0	30.2	49.8	0.98971(3)	1.17627(3)	0.58073(2)
	τ_9	19.9	36.1	44.0	0.40922(1)		1.01504(4)
αRhSi+τ_6+τ_9	αRhSi	0.0	51.2	48.8	0.55456(3)	0.30704(2)	0.63622(3)
	τ_6	19.8	30.6	49.6	0.98862(4)	1.17548(4)	0.58034(2)
	τ_9	19.7	39.8	40.5	0.40848(1)		1.01582(3)
αRhSi+τ_9+τ_{11}	αRhSi	0.0	50.6	49.4	0.55496(2)	0.30721(1)	0.63700(2)
	τ_9	19.2	40.5	40.3	0.40889(1)		1.01657(4)
	τ_{11}	8.4	54.9	36.7	0.69833(2)		0.37833(1)
αRhSi+Rh_5Si_3+τ_{11}	αRhSi	0.0	50.8	49.2	0.55517(3)	0.30707(1)	0.63736(3)
	Rh_5Si_3	0.0	62.6	37.4	0.53181(1)	1.01257(2)	0.38966(1)
	τ_{11}	9.1	54.3	36.6	0.69846(1)		0.37819(1)
Ce_5Si_4+Ce_3Si_2+τ_{17}	Ce_5Si_4	55.4	0.0	44.6	0.79385(3)		1.5072(1)
	Ce_3Si_2	60.0	0.0	40.0	0.77908(4)		0.43690(3)
	τ_{17}	42.6	29.0	28.4	0.56866(3)	0.79739(5)	1.3278(1)
Ce_5Si_4+τ_7+τ_{17}	Ce_5Si_4	55.0	0.0	45.0	0.79438(3)		1.5098(1)
	τ_7	43.0	14.1	42.9	0.41567(2)	0.42595(2)	1.8175(1)
	τ_{17}	42.3	28.6	29.1	0.56840(3)	0.79817(4)	1.32864(6)
τ_7+τ_{10}+τ_{18}	τ_7	42.4	14.6	43.0	0.41553(2)	0.42573(2)	1.81848(8)
	τ_{10}	26.8	36.5	36.7	0.40683(2)	0.41365(2)	2.4462(1)
	τ_{18}	35.8	36.9	27.3	2.0749(1)	0.57242(3) β=110.09(1)°	0.78741(3)
τ_7+τ_8+τ_{10}	τ_7	42.6	14.5	42.9	0.41470(2)	0.42472(2)	1.83269(7)
	τ_8	24.8	34.0	41.2	0.41140(1)	0.41038(1)	1.72547(5)
	τ_{10}	27.4	35.3	37.3	0.40813(2)	0.41322(2)	2.4465(1)
τ_8+τ_9+τ_{10}	τ_8	25.2	36.7	38.1	0.41035(2)	0.41091(2)	1.72633(7)
	τ_9	20.2	40.3	39.5	0.40883(1)		1.01748(2)
	τ_{10}	27.1	36.2	36.7	0.40752(2)	0.41374(2)	2.4466(1)
τ_9+τ_{10}+τ_{18}	τ_9	20.0	40.6	39.4	0.40884(1)		1.01759(2)
	τ_{10}	27.1	36.7	36.2	0.40591(3)	0.41438(3)	2.4464(2)
	τ_{18}	36.2	36.4	27.4	2.0747(1)	0.57210(2) β=110.09(1)°	0.78697(3)
τ_9+τ_{19}+τ_{20}	τ_9	19.8	40.9	39.3	0.40876(1)		1.01765(3)
	τ_{19}	36.9	37.9	25.2	0.77171(3)	1.48725(6)	0.57739(2)
	τ_{20}	24.7	48.9	26.4	0.40568(2)	1.76691(7)	0.40727(2)

Table 8 (*continued*)

Three-phase field	Phase	EPMA (at%)			Lattice parameters (nm)		
		Ce	Rh	Si	*a*	*b*	*c*
$\tau_9+\tau_{12}+\tau_{20}$	τ_9	19.9	40.8	39.3	0.40871(1)		1.01731(2)
	τ_{12}	17.0	49.9	33.1	0.71252(1)	0.97220(2)	0.55932(1)
	τ_{20}	24.7	46.6	28.7	0.40618(1)	1.76413(5)	0.40794(1)
$\tau_9+\tau_{11}+\tau_{12}$	τ_9	20.1	39.8	40.1	0.40892(1)		1.01691(4)
	τ_{11}	9.1	54.6	36.3	0.69899(5)		0.37922(4)
	τ_{12}	17.1	50.0	32.9	0.71273(2)	0.97240(3)	0.55935(2)
$\tau_{11}+\tau_{12}+\tau_{13}$	τ_{11}	9.1	54.6	36.3	0.69881(2)		0.37808(2)
	τ_{12}	16.4	50.4	33.2	0.71268(4)	0.97226(6)	0.55981(4)
	τ_{13}	10.9	54.4	34.7	2.23250(3)		0.38427(1)
$\tau_{12}+\tau_{14}+\tau_{16}$	τ_{12}	16.7	50.4	32.9	0.71289(1)	0.97255(2)	0.55960(1)
	τ_{14}	10.9	54.5	34.6	1.57257(2)		0.38569(1)
	τ_{16}	8.7	62.6	28.7	0.88329(2)		
$Rh_5Si_3+Rh_2Si+\tau_{11}$	Rh_5Si_3	0.0	62.7	37.3	0.53179(1)	1.01235(2)	0.38958(1)
	Rh_2Si	0.0	66.5	33.5	0.54138(1)	0.39286(1)	0.73788(2)
	τ_{11}	9.0	54.8	36.2	0.69853(2)		0.37767(1)
$Rh_2Si+\tau_{11}+\tau_{15}$	Rh_2Si	0.0	66.6	33.4	0.54184(2)	0.39281(2)	0.73812(3)
	τ_{11}	8.7	55.1	36.2	0.69869(2)		0.37820(1)
	τ_{15}	9.2	57.2	33.6	0.97233(3)		0.38448(1)
$Rh_2Si+\tau_{15}+\tau_{16}$	Rh_2Si	0.0	67.2	32.8	0.54257(1)	0.39254(1)	0.73800(2)
	τ_{15}	9.3	57.3	33.4	0.97199(2)		0.38480(1)
	τ_{16}	8.4	62.5	29.1	0.88323(2)		
$Ce_5Rh_4+CeRh+\tau_{19}$	Ce_5Rh_4	54.6	45.4	0.0	0.7486(1)	1.4788(2)	0.7657(1)
	CeRh	49.5	50.5	0.0	0.38528(4)	1.0975(1)	0.41537(4)
	τ_{19}	37.1	38.0	24.9	0.77153(3)	1.48800(7)	0.57637(3)
$CeRh+\tau_{19}+\tau_{21}$	CeRh	49.8	50.2	0.0	0.38786(7)	1.0888(2)	0.41517(7)
	τ_{19}	36.9	38.2	24.9	0.77176(6)	1.4874(1)	0.57599(5)
	τ_{21}	24.7	50.1	25.2	0.40564(2)		3.5533(3)
$CeRh+\tau_{21}+\tau_{22}$	CeRh	49.1	50.9	0.0	0.38439(7)	1.0946(2)	0.41739(7)
	τ_{21}	24.7	50.6	24.7	0.40498(2)		3.5535(3)
	τ_{22}	32.8	51.7	15.5	0.55577(2)		1.17766(6)
$\tau_{21}+\tau_{22}+\tau_{23}$	τ_{21}	–	–	–	–		–
	τ_{22}	33.5	52.7	13.8	0.55364(2)		1.19249(5)
	τ_{23}	33.4	55.1	11.5	1.5260(2)	0.7539(1)	0.5523(2)
$CeRh+CeRh_2+\tau_{23}$	CeRh	–	–	–	–	–	–
	$CeRh_2$	33.0	60.3	6.7	0.75220(5)		
	τ_{23}	33.4	58.2	8.4	1.5431(2)	0.7531(1)	0.5480(1)
$CeRh_2+\tau_{24}+\tau_{12}$	$CeRh_2$	32.6	64.5	2.9	0.75256(2)		
	τ_{24}	23.2	66.5	10.3	0.82524(1)		
	τ_{12}	16.2	50.4	33.4	0.71264(7)	0.9707(2)	0.5591(1)
$\tau_{24}+\tau_{12}+\tau_{16}$	τ_{24}	22.5	67.3	10.2	0.82548(1)		
	τ_{12}	16.8	50.2	33.0	0.71260(2)	0.97160(3)	0.55913(2)
	τ_{16}	8.3	62.8	28.9	0.88242(2)		
$Rh+CeRh_3+\tau_{16}$	(Rh)	0.0	100.0	0.0	0.38011(1)		
	$CeRh_3$	24.3	71.1	4.6	0.40900(1)		
	τ_{16}	8.2	63.0	28.8	0.88225(1)		
$Rh+Rh_2Si+\tau_{16}$	(Rh)	0.0	98.0	2.0	0.38016(1)		
	Rh_2Si	0.0	66.7	33.3	0.54109(1)	0.39294(1)	0.73855(1)
	τ_{16}	8.4	63.3	28.3	0.88266(1)		

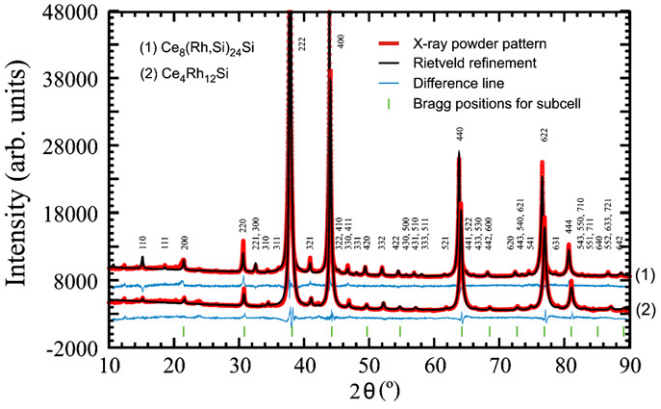

Fig. 4. XPD pattern for samples $Ce_{23.5}Rh_{66.5}Si_{10}$ (1) and $Ce_{23.5}Rh_{70.5}Si_6$ (2) with Rietveld refinement for primitive $Ce_8(Rh,Si)_{24}Si$-type and *bcc* $Ce_4Rh_{12}Si$-type, respectively. Bragg positions are given for the $CeRh_3$ subcell.

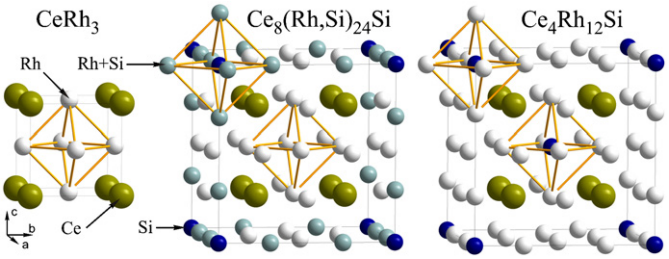

Fig. 5. Increasing Si content starting from binary $CeRh_3$ (Au_3Cu-type, left panel) yields a two-fold superstructure at low Si-contents with *bcc* symmetry ($Ce_4Rh_{12}Si$, right panel) and a primitive cubic structure at higher Si-concentrations ($Ce_8(Rh,Si)_{24}Si$, middle panel) (for details see text).

alloys, which were prepared by various methods employing arc melting under argon or powder reaction sintering. Twenty-seven ternary compounds were detected in the system, and 25 of them

participate in the phase equilibria at 800 °C. Structure prototypes were assigned to nine new Ce–Rh–Si compounds. Phase equilibria are characterized by the absence of cerium solubility in the various rhodium silicides. However, mutual solubilities among cerium silicides and cerium–rhodium compounds are significant.

Acknowledgments

This research is supported by the Austrian National Science Foundation FWF project P18054-Phy. The authors are grateful to the Russian Foundation of Basic Research, project no. 08-03-01072_a, and to the bilateral WTZ Austria–Russia, project 17/06.

Appendix A. Supplementary materials

Supplementary data associated with this article can be found in the online version at doi:10.1016/j.jssc.2010.01.029.

References

[1] R. Ballestracci, C. R. Acad. Sci. Ser. B 282 (13) (1976) 291.
[2] P. Lejay, I. Higashi, B. Chevalier, J. Etourneau, P. Hagenmuller, Mater. Res. Bull. 19 (1) (1984) 115.
[3] P. Haen, P. Lejay, B. Chevalier, B. Lloret, J. Etourneau, M. Sera, J. Less-Common Met. 110 (1–2) (1985) 321.
[4] B. Chevalier, P. Lejay, J. Etourneau, P. Hagenmuller, Mater. Res. Bull. 18 (3) (1983) 315.
[5] B. Chevalier, P. Lejay, J. Etourneau, P. Hagenmuller, Solid State Commun. 49 (8) (1984) 753.
[6] B.I. Shapiev, Interaction of the elements and properties of the alloys in the ternary sustems Ce–{Ru, Rh}–{Si, Ge}, Ph.D. Thesis, Moscow State University, 1993.
[7] A.I. Tursina, A.V. Gribanov, Y.D. Seropegin, O.I. Bodak, J. Alloys Compd. 367 (1-2) (2004) 142.
[8] A.I. Tursina, A.V. Gribanov, Y.D. Seropegin, Acta Crystallogr. E 57 (7) (2001) i55.
[9] Y.M. Prots, J. Stepien-Damm, P.S. Salamakha, O.I. Bodak, J. Alloys Compd. 256 (1–2) (1997) 166.
[10] A.I. Tursina, A.V. Gribanov, Y.D. Seropegin, A.A. Novitskii, O.I. Bodak, J. Alloys Compd. 367 (1–2) (2004) 146.
[11] A.I. Tursina, A.V. Gribanov, Y.D. Seropegin, 2010, to be published.
[12] K. Cenzual, B. Chabot, E. Parthe, Acta Crystallogr. C 44 (2) (1988) 221.
[13] R.E. Gladyshevskii, K. Cenzual, E. Parthé, J. Alloys Compd. 189 (2) (1992) 221.
[14] N. Kimura, Y. Muro, H. Aoki, J. Phys. Soc. Jpn. 76 (5) (2007).
[15] N. Aso, H. Miyano, H. Yoshizawa, N. Kimura, T. Komatsubara, H. Aoki, J. Magn. Magn. Mater. 310 (2, Part 1) (2007) 602.
[16] N. Kimura, K. Ito, H. Aoki, S. Uji, T. Terashima, Phys. Rev. Lett. 98 (19) (2007) 197001/1.
[17] Y. Muro, M. Ishikawa, K. Hirota, Z. Hiroi, N. Takeda, N. Kimura, H. Aoki, J. Phys. Soc. Jpn. 76 (3) (2007) 033706.
[18] T. Shimoda, Y. Okuda, Y. Takeda, Y. Ida, Y. Miyauchi, T. Kawai, T. Fujie, I. Sugitani, A. Thamizhavel, T.D. Matsuda, Y. Haga, T. Takeuchi, M. Nakashima, R. Settai, Y. Onuki, J. Magn. Magn. Mater. 310 (2) (2007) 308.
[19] T. Terashima, Y. Takahide, T. Matsumoto, S. Uji, N. Kimura, H. Aoki, H. Harima, Phys. Rev. B 76 (5) (2007) 054506.
[20] T. Terashima, M. Kimata, S. Uji, T. Sugawara, N. Kimura, H. Aoki, H. Harima, Phys. Rev. B 78 (20) (2008) 205107.
[21] C. Godart, L.C. Gupta, M.F. Ravet Krill, J. Less-Common Met. 94 (1) (1983) 187.
[22] B.H. Grier, J.M. Lawrence, V. Murgai, R.D. Parks, Phys. Rev. B 29 (1984) 2664.
[23] S. Quezel, J. Rossat-Mignod, B. Chevalier, P. Lejay, J. Etourneau, Solid State Commun. 49 (7) (1984) 685.
[24] R. Movshovich, T. Graf, D. Mandrus, J.D. Thompson, J.L. Smith, Z. Fisk, Phys. Rev. B 53 (13) (1996) 8241.
[25] R. Settai, A. Misawa, S. Araki, M. Kosaki, K. Sugiyama, T. Takeuchi, K. Kindo, Y. Haga, E. Yamamoto, Y. Onuki, J. Phys. Soc. Jpn. 66 (8) (1997) 2260.
[26] H. Abe, H. Kitazawa, H. Suzuki, G. Kido, T. Matsumoto, J. Magn. Magn. Mater. 177–181 (Part 1) (1998) 479.
[27] H. Mori, N. Takeshita, N. Mori, Y. Uwatoko, Physica B 259–261 (1999) 58.
[28] T. Muramatsu, S. Eda, T.C. Kobayashi, M.I. Eremets, K. Amaya, S. Araki, R. Settai, Y. Onuki, Physica B 259–261 (1999) 61.
[29] S. Kawarazaki, M. Sato, Y. Miyako, N. Chigusa, K. Watanabe, N. Metoki, Y. Koike, M. Nishi, Phys. Rev. B 61 (6) (2000) 4167.
[30] S. Araki, R. Settai, T.C. Kobayashi, H. Harima, Y. Onuki, Phys. Rev. B 64 (22) (2001) 224417/1.
[31] S. Araki, M. Nakashima, R. Settai, T.C. Kobayashi, Y. Onuki, J. Phys.: Condens. Matter 14 (21) (2002) L377.
[32] M. Ohashi, G. Oomi, S. Koiwai, M. Hedo, Y. Uwatoko, Phys. Rev. B 68 (14) (2003) 144428.
[33] A. Villaume, D. Aoki, Y. Haga, G. Knebel, R. Boursier, J. Flouquet, J. Phys.: Condens. Matter 20 (1) (2008) 015203.
[34] B. Chevalier, P. Rogl, K. Hiebl, J. Etourneau, J. Solid State Chem. 107 (2) (1993) 327.
[35] D.T. Adroja, B.D. Rainford, J. Magn. Magn. Mater. 119 (1–2) (1993) 54.
[36] J.J. Lu, M.K. Lee, Y.M. Lu, L.Y. Jang, J. Magn. Magn. Mater. 311 (2) (2007) 614.
[37] A. Szytula, J. Leciejewicz, K. Maletka, J. Magn. Magn. Mater. 118 (3) (1993) 302.
[38] I. Das, E.V. Sampathkumaran, J. Magn. Magn. Mater. 137 (3) (1994) L239.
[39] J. Leciejewicz, N. Stüsser, A. Szytula, A. Zygmunt, J. Magn. Magn. Mater. 147 (1-2) (1995) 45.
[40] T. Nakano, K. Sengupta, S. Rayaprol, M. Hedo, Y. Uwatoko, E.V. Sampathkumaran, J. Phys.: Condens. Matter 19 (32) (2007) 326205.
[41] S. Patil, K.K. Iyer, K. Maiti, E.V. Sampathkumaran, Phys. Rev. B 77 (9) (2008) 094443.
[42] M. Szlawska, D. Kaczorowski, T. Plackowski, L.D. Gulay, Acta Phys. Pol. A 115 (1) (2009) 132.
[43] Y. Muro, S. Takahashi, K. Sunahara, K. Motoya, M. Akatsu, N. Shirakawa, J. Magn. Magn. Mater. 310 (2007) e40.
[44] D. Kaczorowski, in: X International Conference on Crystal Chemistry of Intermetallic Compounds, Lviv, Ukraine, 2007, Book of Abstracts, p. 7.
[45] C. Godart, L.C. Gupta, C.V. Tomy, S. Patil, R. Nagarajan, E. Beaurepaire, R. Vijayaraghavan, J.V. Yakhmi, Mater. Res. Bull. 23 (1988) 1781.
[46] S. Ramakrishnan, N.G. Patil, A.D. Chinchure, V.R. Marathe, Phys. Rev. B 64 (6) (2001) 064514.
[47] T. Graf, M.F. Hundley, R. Modler, R. Movshovich, J.D. Thompson, D. Mandrus, R.A. Fisher, N.E. Phillips, Phys. Rev. B 57 (13) (1998) 7442.
[48] D. Kaczorowski, T. Komatsubara, Physica B 403 (5–9) (2008) 1362.
[49] A.P. Pikul, D. Kaczorowski, Acta Phys. Pol. A 115 (1) (2009) 235.
[50] D. Kaczorowski, Y. Prots, U. Burkhardt, Y. Grin, Intermetallics 15 (3) (2007) 225.
[51] D. Kaczorowski, in: 16th International Conference on Solid Compounds of Transition Elements, Dresden, Germany, 2008, Book of Abstracts, p. 312.
[52] STOE WINXPOW (Version 1.06), Stoe & Cie GmbH, Darmstadt, Germany, 1999.
[53] Nonius, Kappa CCD Program Package: COLLECT, DENZO, SCALEPACK, SORTAV, Nonius BV, Delft, The Netherlands, 1998.
[54] G.M. Sheldrick, Acta Crystallogr. A 46 (1990) 467.
[55] SHELXL-97. Program Crystal Structure Refinement, University of Gottingen, Germany, 1997.
[56] J. Rodriguez-Carvajal, in: Satellite Meeting on Powder Diffraction of the XV Congress of the IUCr, Toulouse, France, 1990, Book of Abstracts, p. 127.
[57] T. Roisnel, J. Rodriguez-Carvajal, in: Proceedings of the European Powder Diffraction Conference (EPDIC7), Mater. Sci. Forum, (2000), Book of Abstracts, p. 118.
[58] E. Parthé, L. Gelato, B. Chabot, M. Penzo, K. Cenzual, R. Gladyshevskii, TYPIX Standardized Data and Crystal Chemical Characterization of Inorganic Structure Types, Springer-Verlag, Berlin, Heidelberg, 1994.
[59] M.V. Bulanova, P.N. Zheltov, K.A. Meleshevich, P.A. Saltykov, G. Effenberg, J. Alloys Compd. 345 (2002) 110.
[60] P. Schobinger-Papamantellos, K.H.J. Buschow, J. Alloys Compd. 198 (1993) 47.
[61] A. Palenzona, F. Canepa, P. Manfrinetti, J. Alloys Compd. 194 (1) (1993) 63.
[62] M.E. Schlesinger, J. Phase Equilib. 13 (1) (1992) 54.
[63] A.V. Morozkin, A.E. Bogdanov, R. Welter, J. Alloys Compd. 340 (1–2) (2002) 49.
[64] A.V. Gribanov, et al., 2010, in preparation.
[65] A.C. Lawson, J.L. Smith, J.O. Willis, J.A. O'Rourke, J. Faber, R.L. Hitterman, J. Less-Common Met. 107 (2) (1985) 243.
[66] R.A. Gordon, F.J. DiSalvo, Z. Naturforsch. B 51 (1) (1996) 52.
[67] T.B. Massalski, H. Okamoto, P.R. Subramanian, L. Kacprzak, Binary Alloy Phase Diagrams, ASM International, Materials Park, OH, USA, 1990.
[68] P. Villars, L.D. Calvert (Eds.), Pearson's Handbook of Crystallographic Data for Intermetallic Phases, ASM, Meterials Park, OH, USA, 1991.
[69] O. Sologub, P. Salamakha, G. Bocelli, C. Godart, T. Takabatake, J. Alloys Compd. 312 (1–2) (2000) 172.
[70] A. Raman, J. Less-Common Met. 26 (2) (1972) 199.
[71] G.L. Olcese, J. Less-Common Met. 33 (1) (1973) 71.
[72] J. Le Roy, J.-M. Moreau, D. Paccard, E. Parthé, Acta Crystallogr. B 33 (8) (1977) 2414.
[73] A. Raman, J. Less-Common Met. 48 (1) (1976) 111.
[74] A.E. Dwight, R.A. Conner Jr., J.W. Downey, Acta Crystallogr. 18 (5) (1965) 835.
[75] F. Canepa, M. Minguzzi, G.L. Olcese, J. Magn. Magn. Mater. 63–64 (1987) 591.
[76] H. Ghassem, A. Raman, Z. Metallkd. 64 (3) (1973) 197.
[77] E.V. Sampathkumaran, L.C. Gupta, R. Vijayaraghavan, J. Magn. Magn. Mater. 31–34 (1) (1983) 413.
[78] T. Mihalisin, A. Harrus, S. Raaen, R.D. Parks, J. Appl. Phys. 55 (6) (1984) 1966.
[79] I.R. Harris, M. Norman, W.E. Gardner, J. Less-Common Met. 29 (3) (1972) 299.
[80] S.K. Malik, S.K. Dhar, R. Vijayaraghavan, Pramana 22 (3–4) (1984) 329.
[81] L. Schellenberg, J.L. Jorda, J. Muller, J. Less-Common Met. 109 (2) (1985) 261.
[82] I. Engström, Acta Chem. Scand. 19 (1965) 1924.
[83] Y. Muro, D. Eom, N. Takeda, M. Ishikawa, J. Phys. Soc. Jpn. 67 (10) (1998) 3601.
[84] M.B.T. Tchokonte, P.D. du Plessis, A.M. Strydom, Solid State Commun. 117 (5) (2001) 321.
[85] A. Krimmel, M. Reelmis, A. Loidl, Appl. Phys. A 74 (2002) S695.
[86] C. Godart, C.V. Tomy, L.C. Gupta, R. Vijayaraghavan, Solid State Commun. 67 (7) (1988) 677.
[87] B. Chevalier, J. Etourneau, J. Rossat Mignod, R. Calemczuk, E. Bonjour, J. Phys.: Condens. Matter 3 (12) (1991) 1847.
[88] A. Gribanov, A. Yatsenko, Yu. Seropegin, J. Kurenbaeva, N. Kocherov, O. Bodak, Visnyk Lviv Univ. Ser. Chim. 39 (2000) 96.